Aalto University
School of Engineering

Juha-Matti Isomaa

SLIP PROPAGATION IN RUBBER ICE CONTACT

Master's thesis submitted for partial fulfillment of requirements for the degree of Master of Science in Technology, Espoo, 5 May, 2014.

Supervisor **Professor Sven Bossuyt**

Advisor **Ari Tuononen, D.Sc. (Tech.)**

Aalto University
School of Engineering

Aalto University, P.O. BOX 11000, 00076 AALTO
www.aalto.fi

Abstract of master's thesis

Author Juha-Matti Isomaa

Title of the thesis Slip propagation in rubber ice contact

Major/minor Machine Design **Code of professorship** Kon-67

Thesis supervisor Professor Sven Bossuyt

Thesis advisor(s) Ari Tuononen, D.Sc. (Tech.)

Date 05.05.2014 **Number of pages** 62+5 **Language** English

Abstract

The purpose of this master's thesis was to study the phenomena occurring during the slip propagation of rubber specimens on ice surfaces. Deeper knowledge about the phenomenology of rubber friction could lead to development for example in friction properties of tires and rubber seals, which would enhance road safety and increase the efficiency of machines.

A linear friction tester of vehicle research laboratory of Aalto University, Mini-Mu-Road, was used for the friction tests. The counter surface for the rubber was ice, formed on a glass plate. Rubber samples were accelerated from rest after a given dwell time and the phenomena occurring in contact area were captured using a high-speed camera, viewing the rubber in contact with the ice through the glass and ice. The recorded video was then analysed by means of digital image correlation to extract time-dependent full-field displacement measurements of the rubber surface.

According to the results, the whole contact area of the rubber does not detach from the counter surface all at once when slip occurs, but the contact detaches first at one edge of the sample and then a detachment front sweeps through the contact area. The frictional force increases until the last part of the sample is detached, after which the friction level drops down to the kinetic friction level. For un-grooved sample, the last part in contact was always at an edge of the sample.

Results show that for the precursors of the harder rubber, the first precursors occur when the first part of the rubber is detached. The second precursor was found when ice started to crack during the friction build-up phase. A logarithmic dependency was found between rubber friction and dwell time. A friction coefficient larger than 1 was found for hard rubber at dwell times above one minute. In these high friction situations the contact between rubber and ice was stronger than the shear strength of ice and the rubber sample started sliding because the ice broke. Increasing the contact pressure lowered the friction coefficient.

The progress of the detachment front could be slowed or even stopped momentarily by texturing the rubber. Using rubber with chequered surface texture, the last part of the rubber in contact was at the centre of the sample, and the static friction was more than twice as high as with un-grooved sample.

The results show that further research into the initiation and propagation of the detachment front and the effects of rubber texturing could show how to increase the performance of rubber goods.

Keywords ice, rubber, high-speed camera, digital image correlation, rubber texturing, precursors, dwell time

Aalto University
School of Engineering

Aalto-yliopisto, PL 11000, 00076 AALTO
www.aalto.fi

Diplomityön tiivistelmä

Tekijä Juha-Matti Isomaa

Työn nimi Luiston kehitys jää-kumi kontaktissa

Koulutusohjelma Konetekniikka

Pää-/sivuaine Koneensuunnittelu **Professuurikoodi** Kon-67

Työn valvoja Professori Sven Bossuyt

Työn ohjaaja(t) Tekniikan tohtori Ari Tuononen

Päivämäärä 05.05.2014 **Sivumäärä** 62+5 **Kieli** Englanti

Tiivistelmä

Tämän diplomityön tarkoituksena oli tutkia kumikappaleen liukuun lähdössä tapahtuvia ilmiöitä jään päällä. Laajempi tuntemus kitkan muodostumisesta kumikappaleissa voisi johtaa kehitykseen esimerkiksi renkaiden ja kumitiivisteiden kitkaominaisuuksissa, mikä parantaisi liikenneturvallisuutta ja nostaisi laitteiden hyötysuhdetta sekä tekisi toiminnoista sulavampia.

Tutkimuslaitteistona käytettiin Aalto-yliopiston ajoneuvotekniikan laboratorion Mini-Mu-Roadia, joka on kehitetty kitkatutkimusta varten. Kitkapintana toimi lasilevyn päälle tehty jää. Kuminäyte kiihdytettiin lepotilasta liikkeelle ja kontaktissa tapahtuvia ilmiöitä kuvattiin suurnopeuskameralla lasilevyn ja jään läpi. Tallennettu suurnopeusvideo analysoitiin digitaalikuvakorrelaation keinoin.

Mittausten perusteella kumikappaleen koko kontaktipinta ei irtoa jäästä kerralla, vaan kontakti irtoaa ensin kappaleen reunalta, jonka jälkeen kontaktin irtoaminen jatkuu ”irtoamisrintamana” kappaleen läpi. Kitkavoima jatkoi nousuaan, kunnes koko kontaktiala oli liu’ussa, jolloin kitkavoima laski liukukitkan tasolle. Irtoamisrintaman viimeinen kontaktikohta oli aina kappaleen reunassa tasaisella näytteellä.

Mittauksissa huomattiin kovemman kumilaadun ensimmäisten prekursorien tapahtuvan samaan aikaan, kun irtoaminen alkaa. Toinen prekursori löydettiin jään rikkoutuessa kumin liikkeellelähdössä. Esipuristusajalle ja kitkavoimalle todettiin logaritminen yhteys. Yli minuutin esipuristusajoilla päästiin selvästi yli kitkakertoimen 1. Tällöin kovemmalla kumilaadulla jään ja kumin kontaktin vahvuus kasvoi suuremmaksi kuin jään leikkauslujuus, ja kumi irtosi liukuun jään rikkoutumisen takia. Kontaktipaineen kasvattamisella huomattiin olevan kitkakerrointa laskeva vaikutus.

Kumin teksturoinnilla irtoamisrintamaa pystyttiin hidastamaan ja osittain jopa pysäyttämään hetkellisesti. Shakkiruutumaisella kuvioinnilla viimeinen kontaktissa oleva kohta saatiin siirrettyä kappaleen keskelle, jolloin lepokitkan arvo saatiin nousemaan yli kaksinkertaiseksi tasaiseen kappaleeseen verrattuna.

Tulokset osoittavat, että kumin irtoamisrintaman ja teksturoinnin lisätutkiminen voisi johtaa kumivalmisteiden suorituskyvyn parantumiseen.

Avainsanat jää, kumi, suurnopeuskamera, kuvakorrelaatio, kumin teksturointi, prekursorit, puristusaika

Acknowledgements

I would like to thank my professor Sven Bossuyt for important support, explanations and proofreading during making of this thesis. I am grateful to my advisor Ari Tuononen for giving me new points of views and guidance. For fun and relaxed working environment, I would like to thank my colleagues at work, especially Arto Niskanen, Antti Kalttonen and Lauri Ahtiainen.

I am thankful to my gorgeous and supportive partner Roosa and I congratulate her for beating me in the competition of graduating first.

I would also like to thank Henry Fordin Säätiö for financing this thesis.

Contents

1 Introduction

Rubber friction plays an important role in various applications. 70% of the rubber consumption is due to tire manufacturing and in that application high friction between tires and road surface in all conditions is strictly related to road safety [**1**] [**2**] [**3**]. On the other hand there are several rubber applications where friction lowers efficiency and causes extra load and wear, such as sealing and windscreen wipers [**4**] [**5**] [**6**]. Therefore full knowledge of how to alter the friction behavior of rubber is important for developing better and safer products.

Friction of rubber is a phenomenon that is widely researched but is still not fully understood [**7**] [**8**]. Rubber as a material has friction behavior that does not follow Coulomb's or Amonton's laws e.g., because of its viscoelastic behavior. In particular, the force of friction is not directly proportional to the applied load nor independent of the apparent area of contact, and that kinetic friction is independent of the sliding velocity [**9**].

Researching the phenomena of friction between rubber and a counter surface is challenging because it is difficult to monitor the behavior of the contact. There are no sensors that could be attached to the contact without affecting the phenomena. The research is therefore mostly done by measuring the forces acting on a rubber sample or on the counter surface [**10**] [**11**]. Since this kind of research does not produce direct information about the occurring phenomena, the theory of rubber friction is still argued.

The friction of ice is another phenomenon that is still not entirely understood [**12**]. It is known that increasing temperature and sliding velocity of object on ice surface decreases friction and it was therefore explained that ice surface melting by frictional heat was the main cause for low friction of ice [**13**]. However, the phenomena on ice surface are challenging to research without affecting the ice surface itself and recent studies show that there might be other major phenomena affecting the ice friction that can even dominate over frictional melting [**12**].

The contact between rubber and ice is mostly of interest to tire developers and researchers. As described earlier the frictional behavior of rubber and ice are partly unknown and non-linear which makes the frictional behavior of contact between these two challenging to master.

In the fast phenomena occurring in transition between static and kinetic friction of polymers, the entire contact area is not detached at the same time but there is a detachment front that initiates at some point on the contact surface and travels across the surface [**14**] [**15**]. There are fronts travelling at different velocities thorough the contact area where frictional connection of micro contacts break. When this detachment front has travelled through the whole contact surface the contact surface starts moving. This has been studied by pressing two transparent PMMA blocks together and aiming a laser beam at the contact area. The contact area is not smooth at the atomic level, so it are the surface roughness peaks that are in contact and there are air gaps between these micro contacts. A laser beam that hits one of these micro contacts maintains its direction since both materials are the same but a laser beam that hits an air gap is deflects as illustrated in Figure 1. Thus, the amount of laser light captured with camera is proportional to true contact area [**15**] [**16**] [**17**].

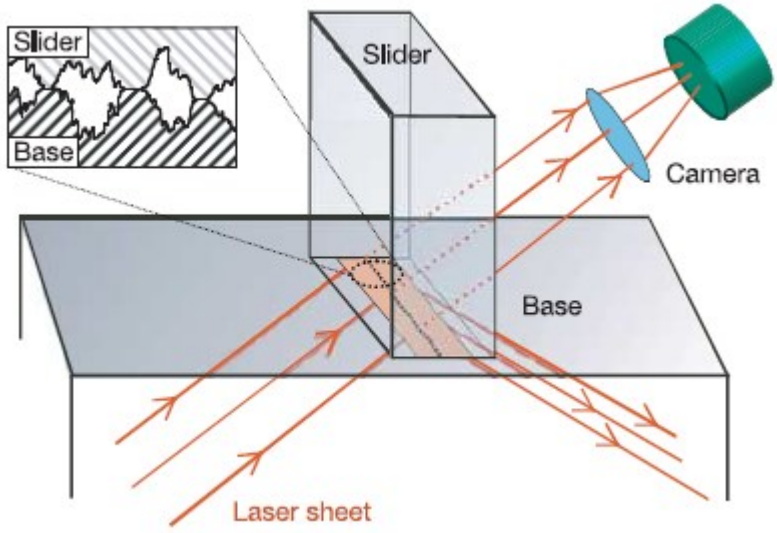

Figure 1 working principle of optical measurement of the true contact area of two PMMA blocks. [15**]**

In addition to this research on the transition between static friction and dynamic friction by optical methods with PMMA [**15**], this transition has been studied mainly by earth-quake researchers with other methods [**18**] [**19**], but better understanding of this phenomenon in rubber could lead to improvements in, and better controllability of, friction properties of rubber for practical applications.

The working principles of devices used for measuring friction in rubber-ice contact are linear movement, rotational movement and in some cases a combination of these two. In machines

using rotational movement, either the rubber sample or the ice is rotating and the other is stationary. Several variations have been reported in the literature such as pin-on-disk, disc-on-disc and drum-type. These machines can be very simple and, because they use small surface area, compact. This means they have good performance and repeatability. However, consequence of this working principle is that the contact point overlaps the same contact where energy is dissipated. This alters the friction behavior of the ice at every rotation. Also these devices' ability to maintain constant speed is criticized [**11**].

Linear movement machines have the opposite advantages and disadvantages to those of rotational movement machines. They are more complex and expensive to build, and require more space, but offer the advantages of better speed control and the possibility to make all the measurements on virgin ice [**11**]. There are also machines that work on mixed linear and rotational movements such as the British pendulum tester [**20**].

The changes in contact area of transparent polymers in the transition between static and kinetic friction have been researched, using laser refraction techniques, by Rubinstein [**15**]. Another optical approach, developed by Tuononen [**14**], is to use a transparent surface such as glass in contact with the rubber sample, and use a high-speed camera to capture fast events in the contact area. It is then possible to calculate the velocity of visible features at the non-transparent sample by digital image correlation-software, and diagnose the behavior of the detachment front. However, there is no mention in the literature of using this method on low friction surfaces, such as ice.

Using Tuononen's approach on ice surfaces it could be possible to study the fast phenomena occurring in rubber-on- ice contact, and perhaps link already-known aspects of the behavior of this contact to those results. This would add general knowledge about behavior of static friction of rubber on ice, which is the purpose of this thesis. This could lead to advanced development of rubber goods. Kinetic friction is not in the scope of this work.

2 Friction of ice and rubber

2.1 Ice

Ice friction theories have evolved many times during history. This is because of the complex processes occurring in contact of ice and because the contact phenomena are challenging to measure directly [**21**]. Different kinds of processes in the contact area that affect friction may occur, depending of the sliding parameters and materials [**22**] [**23**].

The first explanation of ice friction was made by James Thomson in 1850. He suggested that the slipperiness of ice is caused by melting of ice under pressure of an object. It was later shown that by this theory it would be possible to skate only if temperature is above -3,5C [**24**].

In 1939 Bowden and Hughes [**13**] suggested that the frictional heat generated in the sliding contact raised the ice temperature leading a thin layer of ice to melt to water. This water layer would act as a lubricant in the contact and therefore lower the friction. In this theory the frictional heat dissipation of the contact was divided between the sliding sample and ice and it was later derived into equation for the friction coefficient of ice. [**25**]

$$\mu = \frac{Ak(T_m - T_0)}{F_n v} + \frac{B(T_m - T_0)}{F_n v^{0,5}} + \mu_m$$

where A is a constant that depends on the contact area, geometry and slider surface, k is the thermal conductivity of the slider, T_0 is the ambient temperature, T_m the melting temperature, F_n the normal load, v the velocity, B the real contact area and μ_m is the contribution of the friction coefficient due to the energy required to melt the ice surface layer [**21**].

This equation suggested that the friction coefficient decreases with increasing sliding velocities and when the temperature approaches the melting point of ice. The theory was later developed further [**26**] assuming that the thin water layer caused by frictional heating was the only source of friction. The viscous shear of the water layer was suggested to be the source of the frictional force. In this theory transient heat conduction into the slider and ice was taken into account too. This way the theory could predict frictional behavior also when the temperature difference between bulk ice, surface and slider was high. Also the velocity dependence was different for ice close to its melting point and for ice at low temperature. In case of even temperatures between bulk ice, contact surface and the sliding block, the viscous

shear of water played the dominant role and the friction coefficient was proportional to square root of velocity ($v^{0,5}$). However, when the temperature difference between bulk ice and contact surface was high, the heat developed at the contact surface diffused into the bulk ice causing a "dry" contact. In this case, the friction coefficient was proportional to ($v^{-0,5}$). In other words at low temperatures the frictional heat warms the surface and therefore higher velocity warms the surface faster and decreases friction. At high temperatures, it is the shear force in the water layer, which is proportional to $v^{0,5}$, which is dominant.

Later it was suggested that the softening temperature of the ice is more important in friction than its melting temperature [**27**]. At the softening temperature, the surface shear strength of ice is reduced and ice particles in contact are easily removed by shear so no melting occurs in the contact.

The models made of the previous theories require the values of the real contact area, and the amount, distribution and size of the contact points to be known. This is very problematic because those are nearly impossible to measure. Other factor that these models lack is the effect of ploughing, which may play some role in real frictional resistance.

The most recent studies [**28**] [**12**] suggest that the melting of ice does not play a dominant role in ice friction. In these theories the properties of asperity-asperity contacts between ice and counter material define the properties of the contact. Deformation of asperities and scratching of the ice are the main sources of friction, while small-scale melting may occur in the asperity peaks that are in contact long enough to warm above the melting point. The formed water escapes to valleys of the surface roughness. The velocity dependence of friction is therefore explained by changes in ice and counter material strengths.

It was also suggested that at low temperatures ($T < -20C$) and low sliding speeds ($v < 10^{-6}$ m/s) ice sintering starts to increase friction [**29**].

Ice in nature, depending on conditions, has many different forms, such as snow, hail, firn, glaciers and sea ice. The density range of different kind of ices varies from 100-200 kg/m^3 for fresh snow to 900 kg/m^3 for fully dense ice blocks. It is a granular material and exists almost always in the hexagonal structure in nature [**30**]. Ice changes its properties during its life time. Grain growth and dynamic recrystallization are slow changes that happen on a time scale of a few days, while sublimation and deposition of ice moisture are constant processes that happen at the surface of the ice. Sublimation and freezing of moisture are dependent processes since

vapor created by sublimation can be frozen back to the ice surface close to the sublimation point. Sublimation creates pits or “chimneys” to ice while freezing of air moisture alters the surface or ice by creating frost [**12**]. Typical grain structure and frost can be seen in Figure 2.

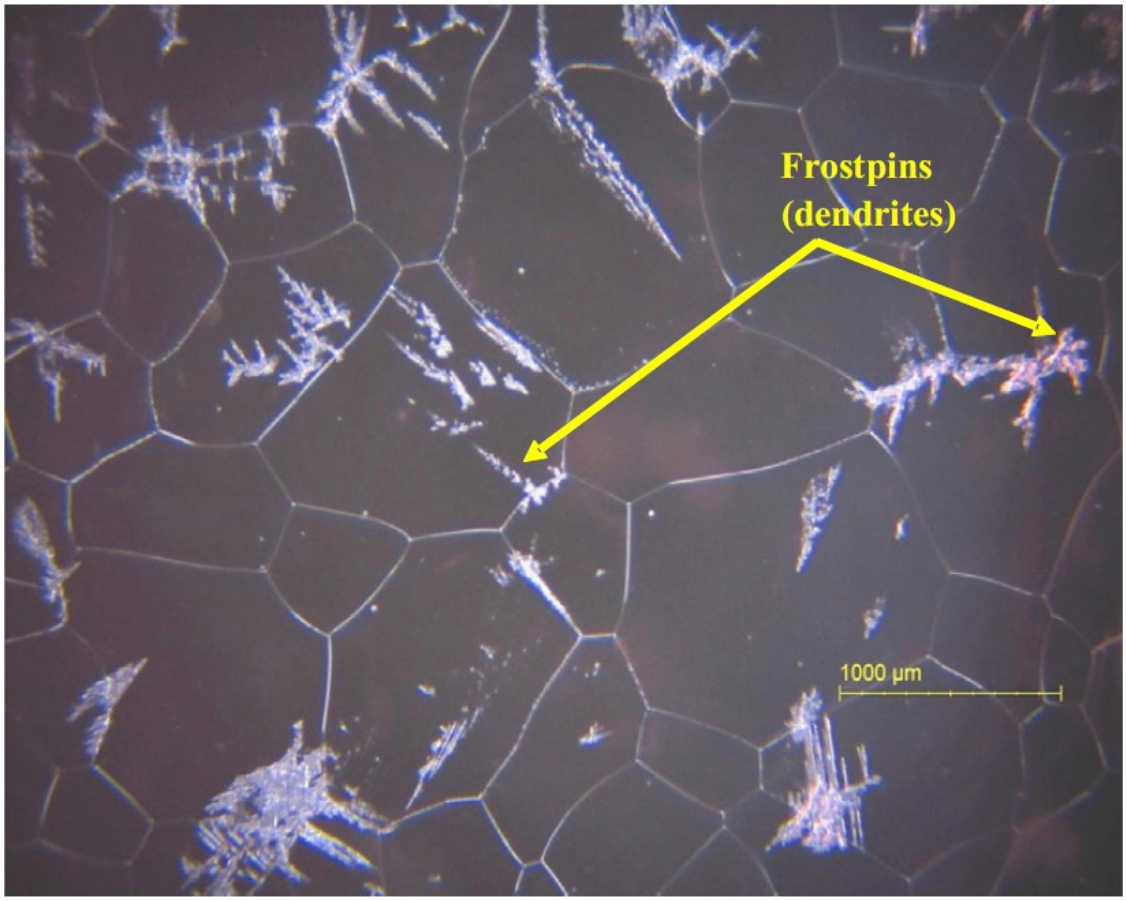

Figure 2 A typical grain structure of ice and small frost spots. [12**]**

At low temperatures ice is hard while near the melting temperature its shear strength drops, as is typical for solid materials [**31**]. The temperature at which ice was formed affects the grain structure. Ice formed at high temperatures tends to form slowly, creating large grains, while high forming speed creates small-grained ice [**32**]. Often in nature ice is found in a columnar pattern because it usually forms by “flooding” on top of old ice surface [**12**]. New layers take the grain boundaries of the previous layers and this structure grows through the thickness of the ice, i.e., epitaxially. This is how the ice of lakes, for example, is formed. The formation speed is affected by the temperature and properties of the surface where ice is created [**32**].

Ice roughness varies depending of the velocity of formation so that quickly formed ice is rougher than slowly formed ice [**33**] [**11**]. The large scale roughness occurs because the heights of the grains of the ice are not equal and small scale roughness is due to surface variations inside a grain. In nature the roughness of ice depends also on previous contacts to the ice. Ice can be roughened by abrasive contacts such as studs in winter tires but also polished by contacts with smooth or elastic material such as shoes or non-studded tires. Figure 3 illustrates the large-scale roughness of a typical ice structure with a columnar pattern.

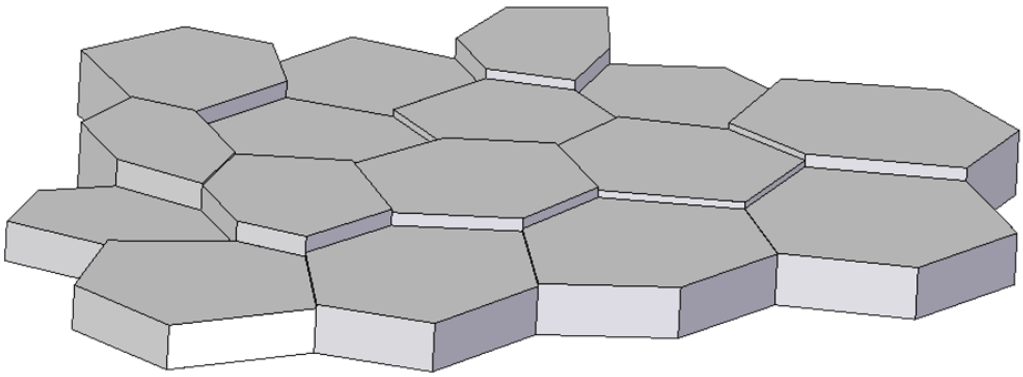

Figure 3 A figure of columnar pattern ice structure.

The ice surface roughness is a major factor considering friction and it creates a problem in researching ice: Repeated contact measurements for virgin ice are hard to perform since the ice surface changes by every contact. After the few first sliding contacts to the surface of the ice, it has smoothened by removal of the loose and weak asperities, plastic deformation, viscoelastic deformation and local melting in contact. This increases the contact area and eliminates the weak particles, leading to higher friction. However, if the sliding contact frequency is high enough, the ice surface heats up, leading to lower friction as can be seen from Figure 4.

Impurities may also affect the behavior of the ice, since dissolved gasses, liquids and solid particles alter the properties of ice [**32**].

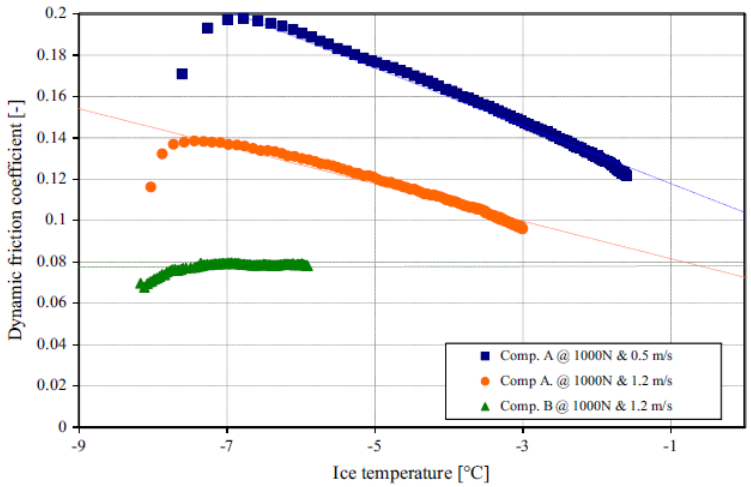

Figure 4 Development of friction level of repeated sliding on the same ice track. At first the friction increases, because the weak asperities of the ice are removed and ice is smoothened. The friction decreases when the same ice lane is ran over many times since the temperature of the ice increases. [12**]**

2.2 Rubber

The most-known characteristic of rubber is its high degree of deformability under the action of comparatively small stresses, typical values for its maximum extensibility are between 500 and 1000 per cent. Rubber does not follow Hooke's law. Its strain-stress curve is non-linear. However, it is possible to define different regions of strain where the stain-stress curve is approximately linear. $2*10^5$ N/mm^2 can be taken as a typical value for the initial Young's modulus at small strains. The relatively low Young's modulus and high elastic extensibility make rubber different from ordinary hard solids [**34**]. A typical strain-stress curve is shown in Figure 5.

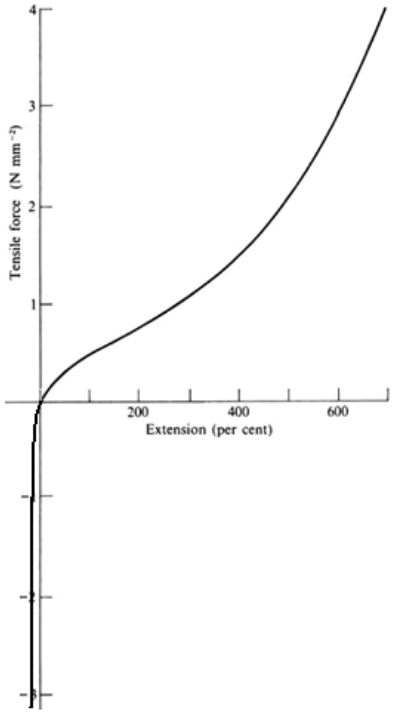

Figure 5 typical strain-stress curve of rubber. Modified from [34**]**

Rubber has also various characteristics that seem counter-intuitive. One of these is the Gough-Joule effect in which rubber (and other elastomers) has a tendency to contract if heated under tension. This process is reversible, so that rubber gives heat out when stretched. Note that this reversible phenomenon is entirely separate from the irreversible phenomena responsible for hysteresis of rubber, that have an important role in rubber friction generated in contact [**35**] [**34**].

Rubber is a polymer, which means that it consists of large molecules that are composed of many repeated subunits. The large molecules are in the shape of a chain, that can have various forms depending on the material. The backbone of the chain consists of singly bonded atoms such as carbon as can be seen in the schematic illustration of the structure of polyethylene in Figure 6. The chains are not actually straight as in Figure 6, but have an angle of about 109 degrees between singly bonded carbon atoms. This angle does not fully define the shape of the backbone since it can be curled in many ways as shown in Figure 7. A polymer chain rarely is at its largest possible length but mostly curled and twisted. Since the single bonds are able to

rotate and bend in three dimensions, polymer chains with single bonds in the backbone can be easily bent and twisted to another shape [**36**].

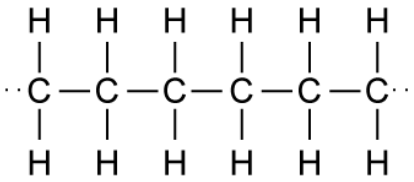

Figure 6 example of the structure of polymer. Here carbon atoms form the backbone. Modified from [37**]**

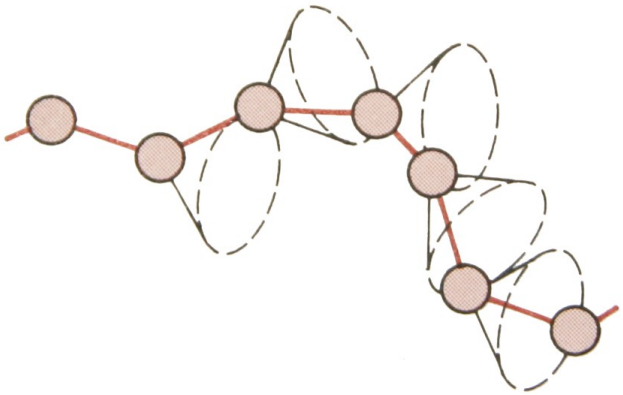

Figure 7 an example of a part of coiled polymer. The red dots represent backbone atoms [36**]**

Polymeric materials, such as rubber, consist of very large number of these polymer chains that are tangled up together. Straining rubber makes these chains uncoil, and since the chains are long and curled in the rest state, rubber can be stretched much more than most materials [**36**]. The restoring force in the elasticity of rubber is due to entropy that decreases when rubber is stretched [**38**]. An open system evolves towards a state where Gibbs free energy is at minimum. The Gibbs free energy is defined by the following equation:

$$G = H - TS$$

, where G is Gibbs free energy, H enthalpy, T temperature and S entropy. If rubber is stretched, the entropy decreases which raises the Gibbs free energy. Therefore a spontaneous reaction to releasing the force is that the rubber contracts back to the original form.

Another interesting behavior of rubber is a phenomenon called the glass transition. At low temperatures and high frequency, rubber does not act like highly elastic material but more like

a glass-like solid. This change does not occur at a precise temperature but gradually over a temperature range [**34**]. In Figure 8 and Figure 9 the elastic modulus and hysteresis of rubber are shown as a function of temperature and loading frequency, respectively. It can be noted that hysteresis increases in the transition phase and elasticity drops at low temperatures and at high loading frequencies.

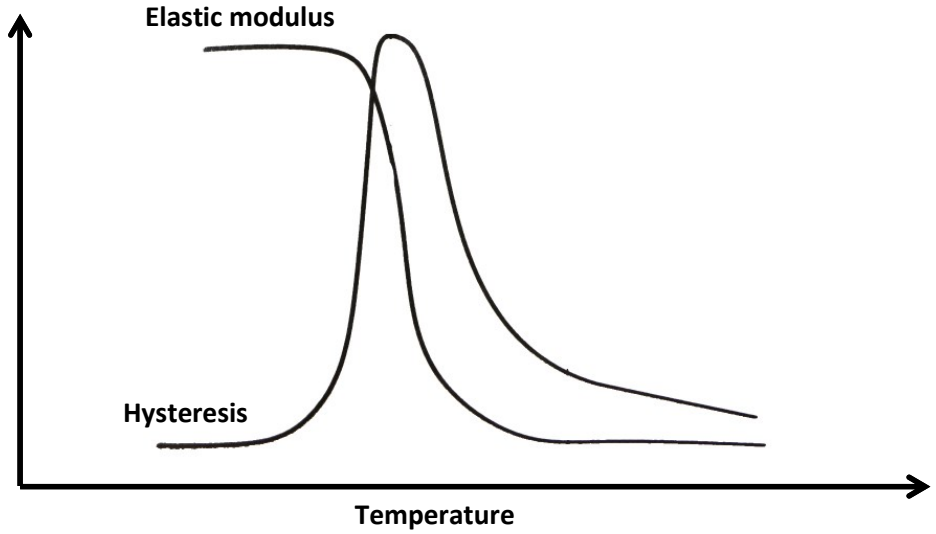

Figure 8 Hysteresis and elastic module of rubber in function of temperature [39**]**

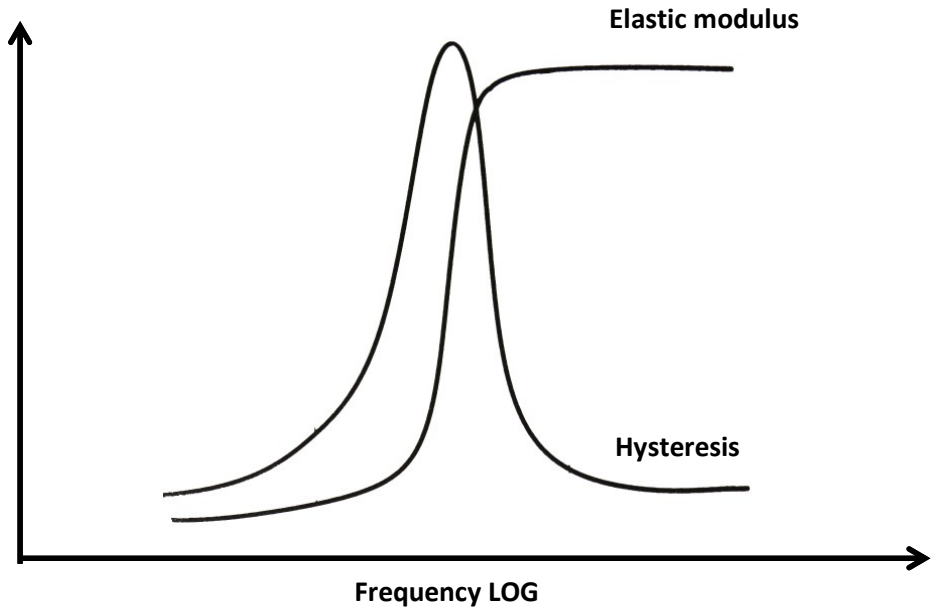

Figure 9 hysteresis and elastic module of rubber in function of frequency [39**]**

The friction properties of rubber differ in many ways from those of other solid materials, because friction of rubber does not follow Coulomb's or Amonton's laws. Amonton's laws state that the friction coefficient is constant and independent of normal load of sliding object, since added contact load increases the contact area with linear dependence. Coulomb's law states that the friction is independent of sliding speed which is not the case of rubber. Friction is in many cases related to the temperature of rubber which affects the elastic modulus and hysteresis of rubber. Increasing temperature raises the friction of rubber to a certain point after which it starts to decrease. It should be noticed that this does not apply if the counter surface is ice since also the properties of ice change depending of the temperature [**40**] [**41**].

The friction between rubber and hard surfaces is caused by adhesion, abrasion and hysteresis. When rubber is sliding over a surface, the roughness of the surface causes oscillating forces to the rubber. This oscillation covers a large range of frequencies because most surfaces have roughness at many wavelengths. The energy that was directed into the rubber by those oscillating forces is partly dissipated into heat in the rubber. This causes a pressure distribution that can be noticed as friction, as seen in Figure 10. The role of adhesion in rubber friction is not as significant as the role of hysteresis and it is arguable whether it plays any role in rubber friction, since adhesive forces start to act at very small distances between rubber and contact surface [**34**] [**40**]. This means that even the slightest impurity could negate this force. However, it cannot be ruled out that on smooth and clean surfaces, adhesion could occur and a possibility is that adhesion helps the rubber to follow the smallest surface roughness. Rubber properties can be altered with fillers such as carbon black to achieve wanted behavior.

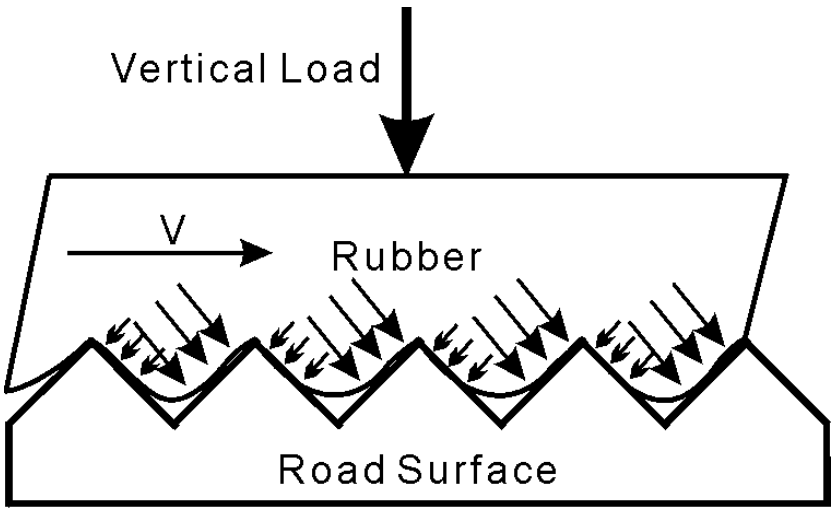

Figure 10 distribution of force of rubber on rough surface. [42**]**

2.3 Ice – rubber –contact

As described above, both ice and rubber have frictional behaviors that do not follow principles of friction of most other solids. The behavior of neither material is totally understood, or at least there is not only one theory that is widely accepted. Also rubber has a high friction coefficient in contact with most materials, whereas ice has low friction. Together these two are considered to have low friction unless there has been a static contact with applied pressure between rubber and ice. These aspects make the investigation of the ice – rubber-contact challenging and interesting.

The true contact area between rubber and ice is another factor that affects the friction. The roughness of the ice or rubber decreases the true contact area and increase contact pressure. Since rubber is a viscoelastic material and ice has significant surface roughness, the true contact area in ice rubber contact is not simply proportional to load but also depends on the dwell time of the load. During the dwell time the rubber conforms to the ice surface better and better, resulting in a larger true contact area and thus higher static friction [**43**].

When the contact starts to slide, the friction level drops from the higher static friction value to lower kinetic friction value. This might be explained by the reduction of true contact area which is the case in PMMA-PMMA –contact. In this case when the sliding initiates the strong contact achieved during the dwell time is lost [**15**] [**17**]. In the sliding motion, rubber cannot take the form of the ice surface as well as when it is loaded against the counter surface for a long time. Sliding also causes frictional heating, which may melt some of the contact asperities causing lower friction [**12**]. A typical friction curve of a rubber sample sliding over ice can be seen in Figure 11. In this figure the rubber sample accelerates from rest to velocity of 500 mm/s. The friction coefficient is calculated by dividing the shear force by the normal load.

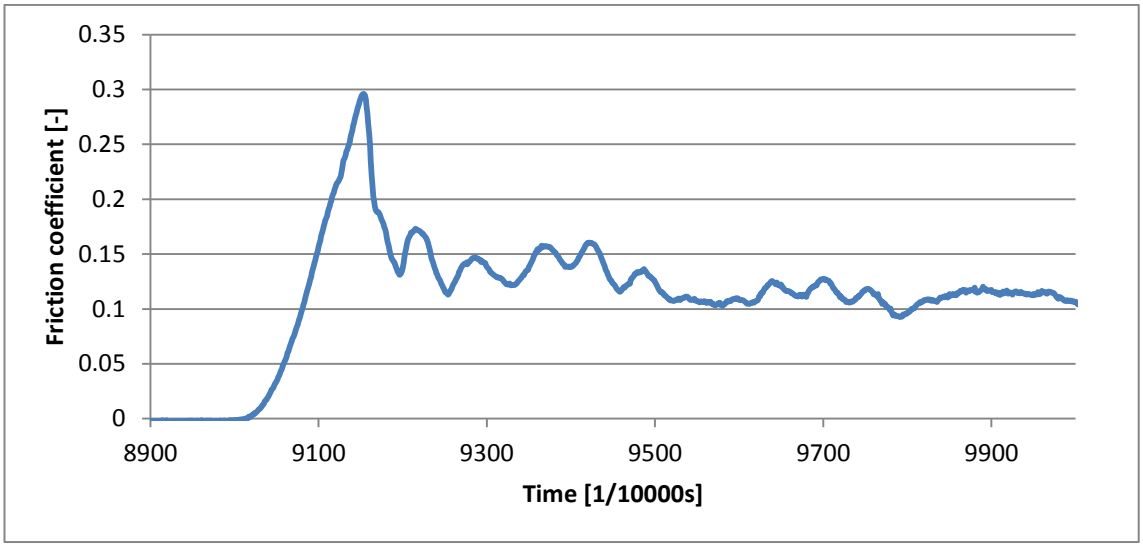

Figure 11 typical friction of rubber on ice contact measured during the tests. A clear drop in friction can be noticed after the build-up phase. The drop is followed by fairly constant friction level.

The areas of the contact that do not melt in sliding motion are prone to abrasion. The surface roughness peaks of rubber extract ice material, which requires energy that is experienced as friction. The frictional heating leads to higher temperature of the surface, which makes the ice softer, which can lead to easier removal of material [**12**].

With some sliding parameters and rubber materials there may occur a phenomenon called stick-slip. In this phenomenon a part of the contact sticks to the ice while other parts of the rubber are still sliding. The stuck part then slips, only to stick again. This causes a 500 Hz – 1000Hz vibration in the rubber, which can be heard as the squeal of tires [**14**] [**44**].

At very low ($<10^{-4}$ m/s) sliding speed there may not be true sliding rubber ice-contact, but the motion between two surfaces occurs due to Schallamach waves. Schallamach waves occur when rubber is folded in the contact and forms “ridges” that travel through the contact area so that locally the rubber is not in contact with the ice [**44**].

3 Digital Image Correlation

Digital image correlation (DIC) is a method that is used to examine changes between two or more images. The same kind of technique has been used widely for determining changes or progress in other kind of datasets and it became a research tool for digital images in 1960's after the digital image camera invention. Progress in the performance of digital cameras and computer calculation speed has led to steadily increasing performance of DIC, which is currently used in many areas of engineering. Most commonly, DIC is used in mechanical testing that includes measurements of deformation, displacement, strain and optical flow [**45**].

The basic idea of DIC is that two images are compared and the changes in the images are explained by the effect of applying a deformation to the image, as calculated with a computer. Determining the movement between pictures cannot be done by searching for a single pixel with matching gray scale value, since an image consists of many pixels with the same gray scale value. Therefore a small group of pixels, called a subset, is selected for the DIC software to be searched between images. Figure 12 shows an example of DIC for sequence of seven images. The yellow area in the first image is the subset that the program tries to locate in the next images, while allowing that the subset can be distorted or rotated. When the program finds correlating subsets, the translation of the center of the subsets can be calculated and this is taken as the displacement field measurement at that location [**46**].

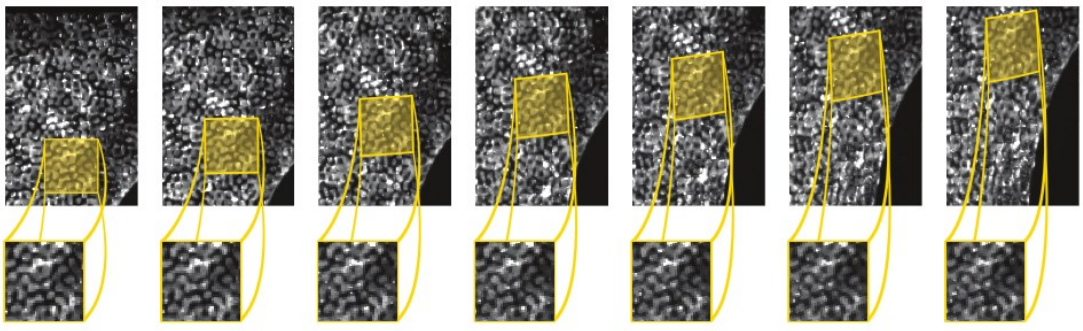

Figure 12 Example of DIC. The subset of first image is detected from other images. [47**]**

If the scale of the images is known, then the deformation in pixels can be converted into deformation in length units, and if the time elapsed between images is known the program can calculate the speed.

The fact that the method is independent of the imaging technology used and can therefore leverage the wide variety of existing imaging technologies is the greatest advantage of DIC. In the simplest case, the measurements can be performed by simply recording a sequence of photographs of the event that is to be studied, and then analyzing the sequence with DIC. Since the data is collected by capturing the light emitted or reflected from the measured object, the phenomenon that is being measured is not affected by the measurement [**45**].

The challenge of the measurement is that its accuracy depends of the quality of the images and the visual patterns of the measured surface. DIC needs some kind of contrast in the image to find changes. A shiny homogenous surface exhibits no chances between the images inside the homogenous area, so DIC will not be useful. Specular reflections of light in the measured area can cause the same effect [**46**].

To overcome the problem with homogenous surfaces the surface can be machined, painted with a pattern or dusted with powder. In recent years the patterns to be applied to surfaces have been developed further to maximize the accuracy of DIC.

A good pattern for the surface of the measured item is an isotropic speckle pattern. This means that the pattern does not have a preferred orientation and therefore all in-plane changes in the image are noticeable. An example of a good pattern can be seen in Figure 13. A pattern that repeats is not good for DIC, since a displacement by the repeat distance would not be detectable from image [**46**] [**48**].

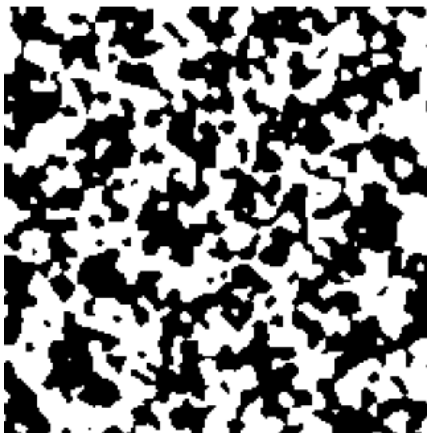

Figure 13 an example of good speckle pattern. It has a random small scale pattern and high contrast [48**]**

4 Test methods

The tests are performed in the cold chamber of Vehicle engineering research group at Aalto University. The cold chamber is constructed to keep even temperatures and humidity at the range of temperatures used in this study. The steadiness of the temperature and the humidity are essential for the ice-friction tests since the properties of ice are strongly dependent on these parameters. The cold chamber temperature is kept at -5C or -12C depending on the measurements made [**11**].

A linear friction tester especially designed for low friction testing is chosen to perform the tests. In this device, called Mini-Mu-Road, the rubber sample is fixed to a sledge that controls the movement and vertical load of the sample. It also measures the normal load and shear force on the sample.

The ice surfaces for the tests are prepared by a flooding technique. A thin layer of distilled water is frozen layer by layer on a glass plate, until the desired ice thickness is achieved. The grain size with this method is between 1 mm and 2 mm. The rubber sample is loaded against the ice surface and after the dwell time a forward movement is initiated. That both the glass plate and the ice layer are transparent, makes it possible to collect visual information from the contact surface.

For visually studying the fast phenomenon of friction changes from static to dynamic, a high-speed camera is fixed under the machine to film the contact area. From the video it is then possible to calculate the speeds of different parts of the rubber sample at the beginning of detachment, using software called DaVis. This data, together with the friction data collected with Mini-Mu-Road are then examined.

4.1 MMR

Mini-Mu-Road (MMR) is a linear friction tester in the vehicle research laboratory at Aalto University. It is specially designed for measuring friction forces of rubber samples and low-friction surfaces at temperatures below 0C, and for its operation it is placed in a cold chamber. It has been used in several studies concerned with rubber friction, ice friction properties or

properties of rubber-ice contact [**11**] [**14**] [**49**]. It has been built in 2001 and been upgraded several times during its service.

The frame of the machine is made of aluminum profiles that are fixed to a table where the sliding surface is installed. Over that table are a frame for a linear guide and supports for electric cables and pneumatic tubes. A sledge that moves the samples is fixed to the linear guide. The sledge consists of an "L" shaped frame to which the sample holder is fixed via four-bar linkage. This way, the sample holder keeps its orientation through vertical movements. The sample holder is vertically connected to the sledge frame by a pneumatic cylinder. The sample holder is spring locked to allow quick sample switching between runs. A spring attached between a link of the four bar linkage and the sledge frame holds the sample holder in its upper position when there is no pressure in the pneumatic cylinder.

The linear motion is achieved by a linear guide and a servo motor that operates the sledge. Contact pressure is exerted by a pneumatic cylinder providing a normal load to sample. This load is controlled by a digital pressure valve. Piezo electric load cells are used to measure the friction force and the normal force. The linear motor has sensors for position and its derivatives. A LabView program is used for data acquisition and control of the machine. The MMR is shown in Figure 14.

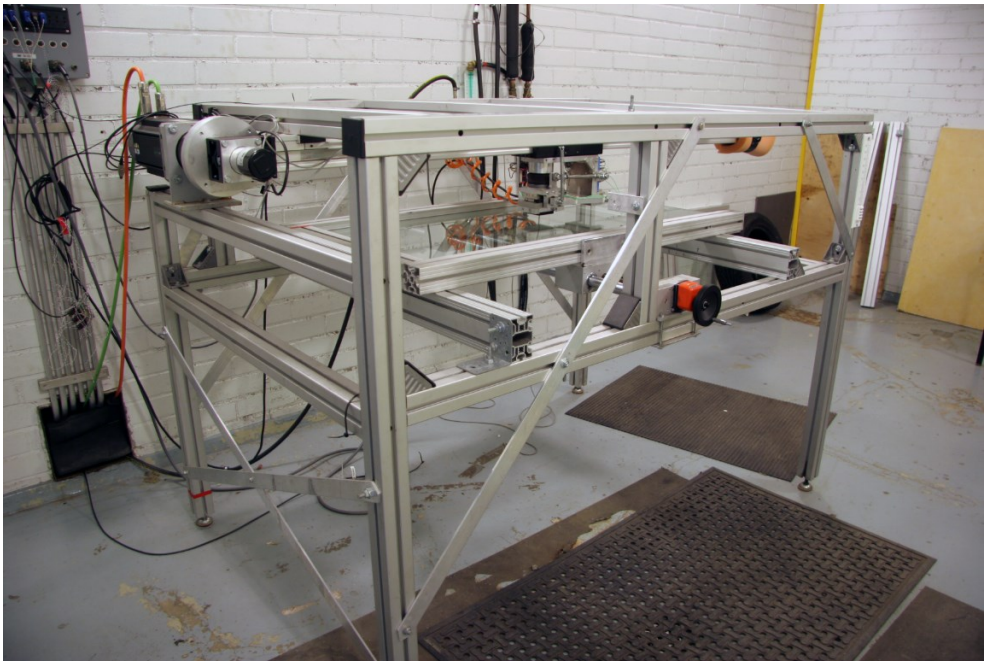

Figure 14 Linear friction tester Mini-Mu-Road

Rubber samples for the MMR are typically 60 mm wide and long, and their thickness is 12 mm. They are glued to metal plates that fit the sample holder. The sliding surface area is typically 500 mm wide and 1200 mm long. Different kinds of surfaces have been used, but the most common ones are asphalt, glass and ice. The sliding lane can be altered in lateral direction by a crank that moves surface plate. The maximum speed of the machine is 2 m/s, the maximum acceleration is 9 m/s^2 and the maximum normal load is 1200 N. Due to high acceleration achievable with the linear motor, it is possible to have high stabilized sliding speeds in short distance, so it is possible to have up to 28 virgin ice lanes on one test plate. This number is reduced if very high sliding speeds are needed.

A typical test for this machine involves a sliding distance of 200 - 300mm with normal load of 800N. This corresponds to a contact pressure of 2,2 bar that is typical for tire pressure.

The test procedure consist of the sample change (if needed), driving the sample to the starting position, lowering the sample and generating the desired vertical load to sample, maintaining the load during the dwell time, and accelerating the sample.

To ensure that the video data from camera and the measurement data of MMR are synchronized, the measuring system has adjustable triggering point. In these measurements the triggering point is located 40 mm behind the starting position of the sliding motion, so that the stabilization of the friction can be seen from the measurement data and it is ensured that all the phenomena affecting the static friction that are visible to the high-speed camera are recorded.

The construction of the sledge can be seen in Figure 15. The piezo sensors are located between the sample holder and the linkage, which results in negative force when the sample is lifted and it is not in contact with sliding surface. This is negated by adding the weight of the sample and sample holder to the vertical force when analyzing the data. The mounting point of the sensors also causes the inertial forces of the sample holder and samples to be added to the measured shear forces. Measurements show maximum inertial force of 25N with the sliding parameters used in this work, when the test is performed without the sample contacting to the sliding surface. This will not be subtracted from the measurement data, since the individual detachments in these tests may result in a different distribution of inertial forces.

The construction of the measuring sledge can be seen in Figure 15 and Figure 16. When the pneumatic cylinder presses the rubber sample against the surface, the four-bar link tilts to an

angle in relation to surface. The force produced by the cylinder is equal to the supporting force of the surface if the sample is not moving. This same force is applied through the force sensors and they show the correct vertical load.

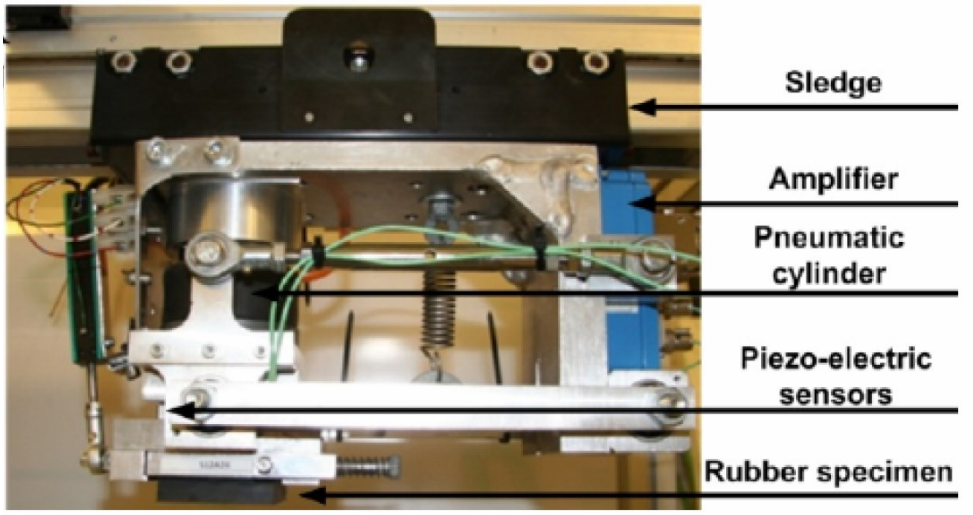

Figure 15 The sledge of MMR. The four linkage keeps the sample parallel to counter surface.

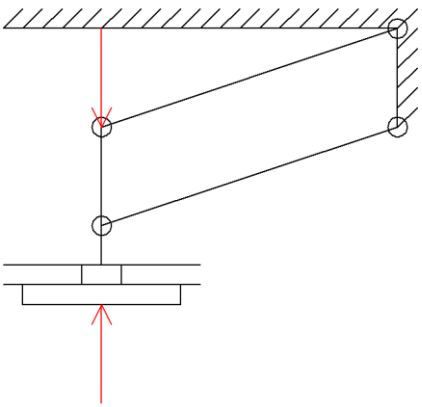

Figure 16 Forces acting to stationary sledge. Only the load of pneumatic cylinder and support force of counter surface are present.

When the rubber sample is moved forward there arises a friction force that acts on the contact area in the opposite direction of sliding. This causes stress to the four bar linkage as shown in Figure 17. The direction of the friction force is not parallel with the four bar linkage direction, so there remains a vertical force that causes a moment in the four bar linkage. In compensation, the supporting force of the surface must lower which causes the contact force to reduce. This means that at the beginning of sliding, the contact force decreases depending

on the friction level. This is decrease can be seen in the measured vertical load data. This may cause some error to the measurements, since the vertical load decreases during the buildup of the friction force, causing possible changes in the connection between rubber and ice.

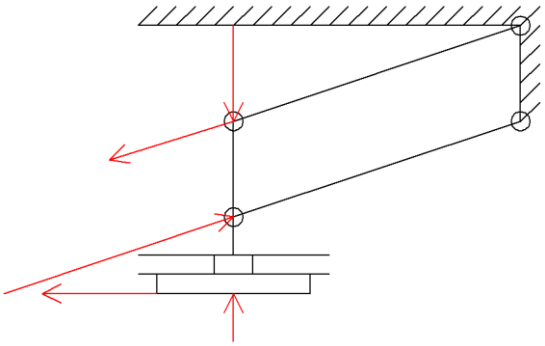

Figure 17 Forces acting to moving sledge. Supporting force of the ice has reduced due to response of structure to frictional force. This decreases slightly the normal load at initiation of sliding motion.

The measured shear force is divided by the measured loading force to achieve normalized friction force. This normalized friction force for all measuring points is referred as friction coefficient in this thesis. The kinetic friction coefficient refers to stable friction level on stabilized sliding situation and the static friction coefficient refers to the highest friction level gained when there is an undetached point of contact on contact area.

4.2 DaVis

The program used in this work to perform digital image correlation is La Vision's Data Acquisition and Visualization software, DaVis 8.1. The tool to calculate the wanted speeds from the contact area is called StrainMaster.

The recorded video is saved in .tif-format and uploaded to the software. The program calculates the changes of the pixels and it is possible to convert the movement of the pixels to real-world coordinates with a scaling image. Figure 18 shows the scaling image that was used for the tests. The scaling image is taken from millimeter grid paper that is placed on top of the test ice. Two pixels of the image are selected and the distance between these is given to the software. The selected pixels had distance of 30mm in direction of x-axis of the grid and 40mm in in direction of y-axis of the grid. It should be noted that the scale is constant for the whole picture area which might result a small scale error on the edges of the photo, depending on the objective and distance from camera to the paper.

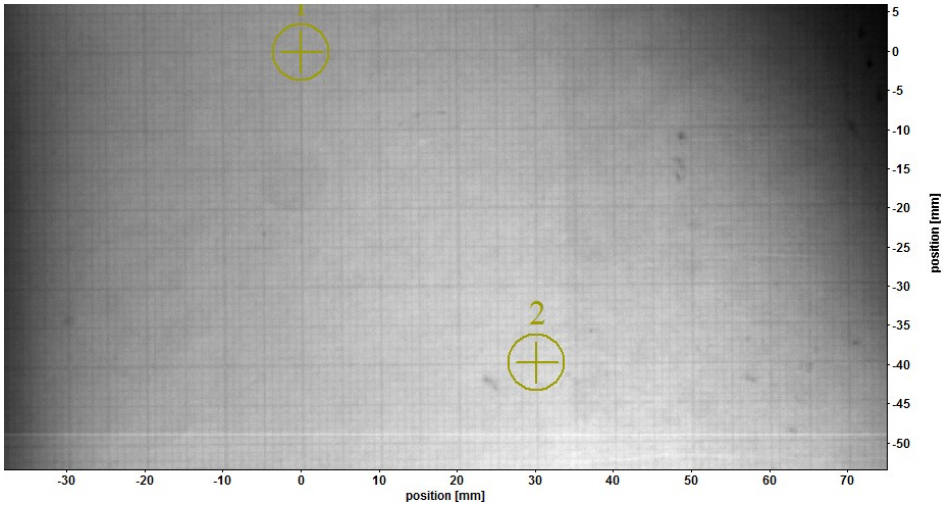

Figure 18 The scaling image. The distance between two selected points is given to software.

The software requires the time difference between images to calculate the velocity field of the rubber. During processing it is possible to change other properties of the images to make it visually more informative and crop the videos. The cropping is important when calculating either long videos or a large number of smaller videos, since the calculation process requires a lot of calculating power and time.

The calculation can be made faster by adding a mask to the image that crops the area of calculations to the interesting area. The mask of the data for this work is shown in Figure 19. It is the larger blue box that is drawn few millimeters inside the edges of the contact area. This way the calculations are only made on the contact area and not the area that was exposed due to bending of the rubber.

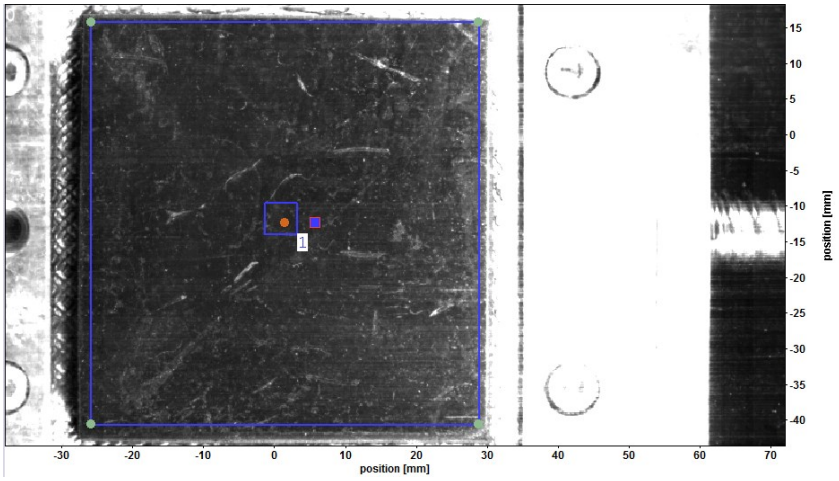

Figure 19 Masking the data. The larger blue square is the mask which is just smaller that the contact area to avoid errors caused by flexing of the edges of the samples.

DIC measures the movement by matching the reference subsets of the first image with the target subsets in following images. The subset size and seeding point are selected manually for this work. The seeding point is selected to be close to the center and the used subset size that was a little bit larger than the largest featureless “all black” area of the rubber sample. More accurate results might be gathered by more carefully selecting the subset, for example using the “subset entropy for optimal selection of subset size for the DIC”-technique. [**46**]

The program shows the speed of the changes in either as vector arrows or color field corresponding to the velocity of the part of the rubber. An example of the velocity distribution of the sample is shown in Figure 20.

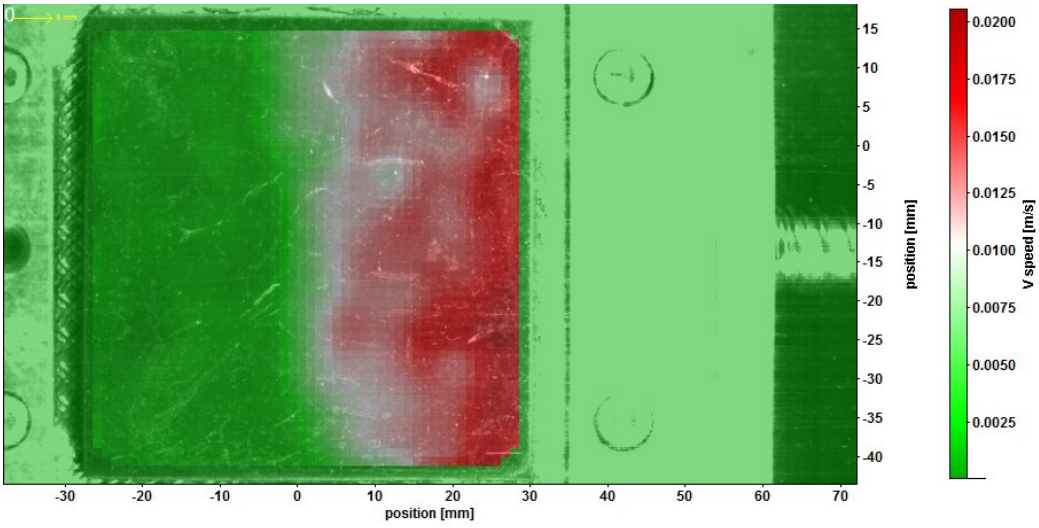

Figure 20 speed distribution calculated by DaVis. Red area is detached and green is still in contact.

4.3 High-speed camera

A high-speed video camera was used in the test to capture the fast phenomena that occur during the change from static to dynamic friction. The phenomena that occur in contact area would be disrupted by using sensors that have to be physically added to the contact area, which makes the studying of the contact challenging with most methods. With the high-speed camera, the visual information can be recorded and then played back at lower speed to enable humans to observe what happens in the contact area. The recorded video can also be analyzed with digital image correlation software to calculate strains or velocities of the objects in the video.

The camera that was used for this study was a Photron Fastcam SA3. Its maximum frame rate (fps) is 120000 and maximum resolution is 1024 x 1024. If a high frame rate is used the resolution must be lowered and vice versa. In this test 5000 fps was used, since it gave acceptable resolution and this speed allowed studying the phenomena with sufficient accuracy. Force data was collected with sample rate of 10 000 Hz so the 5000 fps of the camera made it easy to synchronize recorded videos with measured force data. The high-speed camera is shown in Figure 21.

Figure 21 Photron Fastcam SA3 high-speed camera.

The lens was an AF Micro Nikkor 60mm f/2.8D and an aperture of 1/4 was used to allow the maximum amount of light to enter the sensor since the shutter speed of the camera was 1/5000 s. This made the depth of field rather narrow and fine adjustment of focus became important. Focus of the lens was achieved by focusing to millimeter grid paper placed on the ice surface. The same paper was used to calibrate the DIC-software. When the camera is in recording mode, it starts to record the video to memory. The on-board memory of the camera can only save 1 to 4 seconds of the video, depending on the resolution and frame rate. When that is filled, it overwrites the video in memory with newer video. When it is triggered it will either stop overwriting from the triggering forward, save the most recent half of the video and record over the other half, or overwrite the whole memory once more, depending on the triggering mode that user chooses. The MMR data acquisition ended with a triggering signal to camera so the trigger was selected to be the end point of the video. This way the measured data and video were synchronized.

The high-speed camera was mounted on a camera holder under the glass where the initial position of specimen was. The camera was positioned using bubble level to be pointing in the

vertical direction. A new virgin ice lane was selected by moving the ice plate which, meant that the camera could stay in one position for all the tests and the calibration and refocusing had to be done only in the beginning of each testing day.

The recording was controlled by the Photron fastcam-software. With this software the videos were loaded from the camera, cropped and then saved for further study. This software also sets the triggering mode.

4.4 Rubber samples

An example of the rubber samples used in the Mini-Mu-Road is shown in Figure 22. A water-cut rubber sample with dimensions of 60mm x 60mm x 10mm is glued to an aluminum plate that attaches to the sample holder. The surface where the rubber is glued had been machined with high feed speed to create a grooved surface so that any excess adhesive has a pocket to squeeze into. This allows the rubber to set evenly against the plate, and therefore the contact pressure between rubber sample and counter surface is more even.

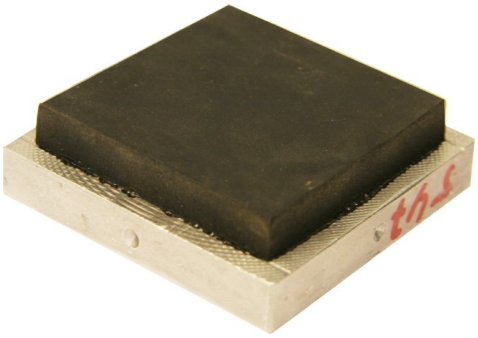

Figure 22 An example of rubber sample. A rubber block is glued to aluminum frame.

The tests were performed with two different rubber materials: the hard one and the soft one. The soft rubber has hardness of 52ShA and the harder one 67ShA. Rubber texturing was performed to the softer sample type: there were one sample with large grooves, one with small grooves and one without grooves as shown in Figure 23. The grooves were cut with a scalpel attached to the chuck of a milling machine and the rubber sample was moved by the vice of the table of the milling machine.

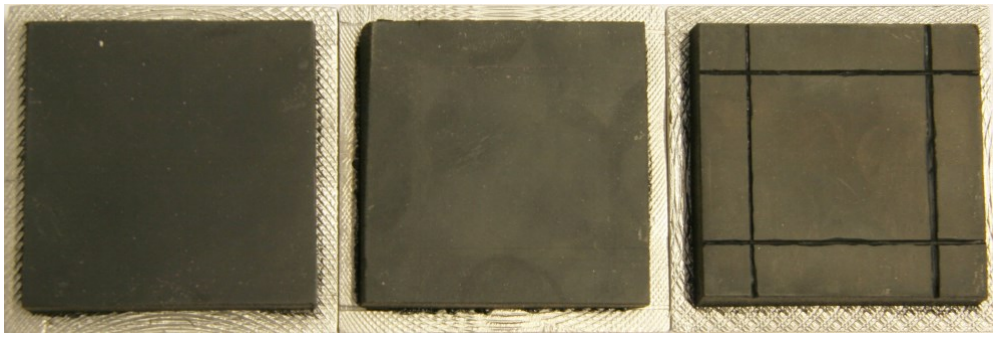

Figure 23 Picture of smooth sample, small-grooved and large-grooved sample from left to right. The small grooved are hard to notice but the pattern is the same as in large-grooved one

A run-in was performed for each of the samples by sliding 20 times with 2 second dwell time and 1000N normal load. This eliminates the Mullins effect and the rubber performs more evenly [**50**]. However, when high dwell times are used, the friction level rises above the forces of the run-in and some error is caused by this effect. The rubber samples were kept in the cold chamber at least a full day to ensure that they were at the same temperature as the chamber.

4.5 Ice preparation

In the Mini-Mu-Road the ice is prepared on an aluminum-framed glass plate in the same cold chamber where all the tests are performed. This way the ice is prepared at the same temperature that is used for the tests and the preparations for each ice plate of similar tests are done at the same temperature. It is notable that the ice sheets for testing different temperatures are prepared at different temperatures, which may affect the comparison between friction at low and high temperatures. Ice also changes its properties over time, so no older than six hour old ice was used in tests. The test day always started with making new test ice.

Preparation of the ice has an important role in the measurements, since the properties of ice play a major role in friction. Preparing ice at different temperatures, from different water, with different technique and tools will result in ices with different frictional properties [**11**]. The variation is not a problem at the scale of just one test ice sheet, since the properties of the ice across one plate remain closely the same. However, preparation with wrong techniques results in macroscopically uneven surfaces which lead to poor results because the shape of the ice dominates the forces generated. Therefore the conditions and the technique of ice making must be identical when ice is made for different plates and at different times. To ensure this,

ice sheets for similar tests are prepared with the same procedure to ensure the comparability of tests done at different times with different ice sheets.

The glass frame and tools are kept in the cold chamber for at least four hours to reach the same temperature as the cold chamber before the ice preparation. The ice is prepared from distilled water to minimize the effect of different kinds of impurities. A small amount of distilled water is poured over the glass plate and moved around the plate with a spatula until almost all water is frozen. After that, more water is poured and this is carried on until 2 to 3 dl of water is frozen. Then the ice is left to cool down, before a new layer of ice is prepared. This procedure produces smooth, transparent and uniform ice sheets that are suitable for testing. The ice thus prepared at -5C has a grain size of 1 mm to 2mm.

The surface of the ice varies not only over time but also depending on the moisture levels of the cold chamber. Therefore it is important to avoid opening the door, since warm air contains more moisture and this moisture is frozen on the surface of the ice.

5 Results and discussion

Tests were divided into two different sessions that had one month gap between them. In the first test the effect of contact pressure, rubber elasticity, temperature and dwell time were studied. Dwell time is the time period during which rubber sample is pressed against the ice surface before sliding motion. In the second test session rubber texturing was studied.

The recorded high-speed video of changes in the contact area has resolution of 768x432 pixels. The video is cropped so that in the direction that is normal to the sliding direction only a few millimeters of data outside of the rubber sample are collected. In the direction of sliding the captured area is longer than the sample to record the first 40 mm of sliding. An example of the recorded area is shown in Figure 24. By cropping the recorded area it was possible to increase the frame rate of the camera to 5000 Hz. In all of the figures the sliding direction is to the right.

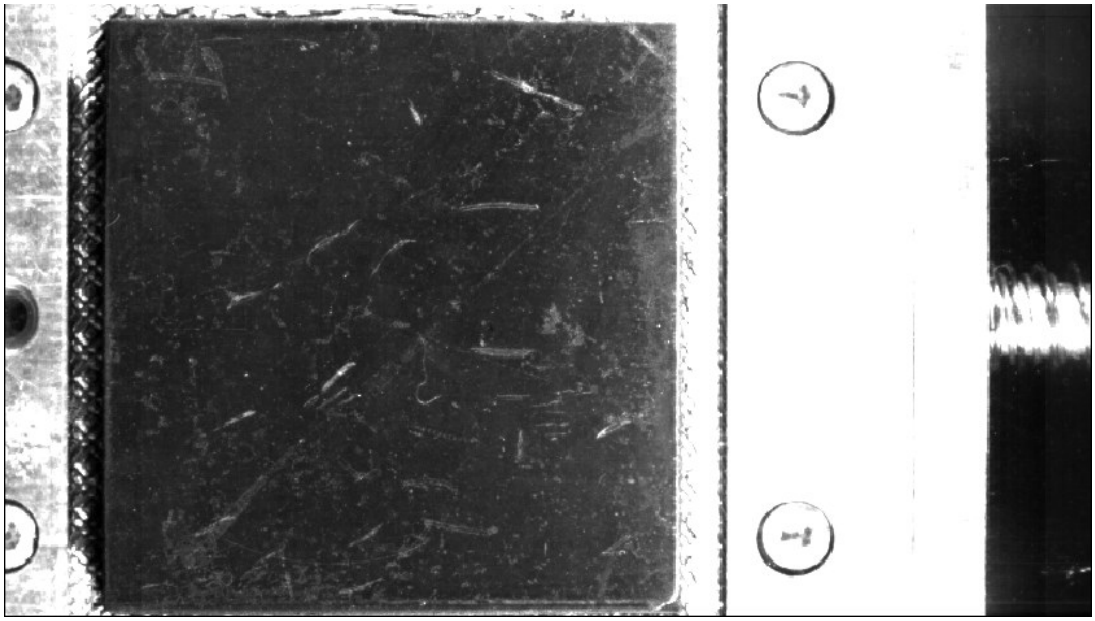

Figure 24 One image of a recorded video

The measured shear force is divided by the measured loading force to achieve normalized friction force. This normalized friction force for all measuring points is referred as friction coefficient in these results. The kinetic friction coefficient refers to stable friction level on stabilized sliding situation and the static friction coefficient refers to the highest friction level gained when there is an undetached point of contact on contact area.

5.1 Slip propagation of un-grooved sample

An example of a set of images of the recorded videos is shown in Figure 25. These images are every tenth frames of recorded video that shows an initiation of sliding. Recoding with 5000 frames per second this means that the time gap between each image is 2 ms and the time from rest to sliding is 6 ms. It is difficult to see any great change between these images even if they represent the detachment of the contact. This test was performed with a short dwell time of 5s and the sliding direction is to right.

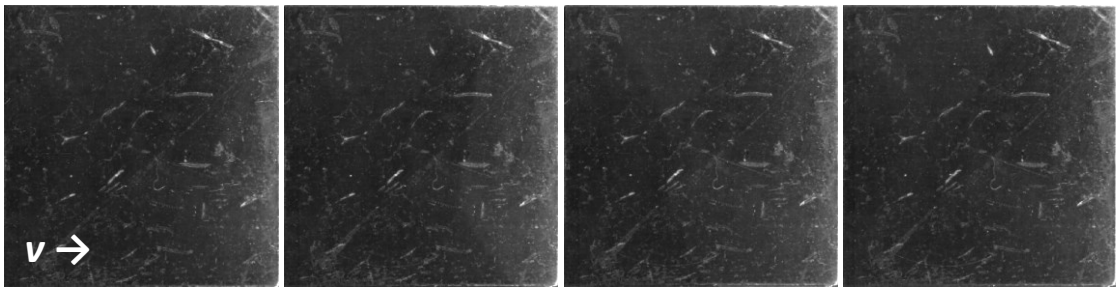

Figure 25 A set of images of a recorded video.

A clearer view of the slip propagation can be obtained for soft samples with the help of digital image correlation, by plotting the velocity distribution. In Figure 26 this is shown for the same frames of video as in Figure 25.

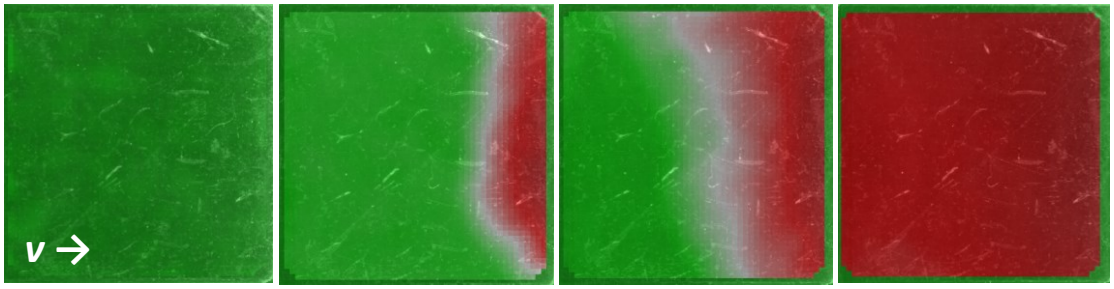

Figure 26 Velocity distribution calculated with DIC

In this figure the areas that move the slowest are represented in green color and the parts that are moving over 20mm/s are represented as red. In the first image, the contact surface is not moving yet, as the whole contact area is green. In the next image, it is clear that the leading edge of the sample has higher velocity than the rest of the sample and therefore it can be stated that the leading edge has detached. It is also possible to see a clear front where the

particles of the rubber change from rest to movement which is called the detachment front. In the third image the detachment has progressed, as the detachment front has moved closer to the trailing edge. Now a gradient of velocity can be noted around the detachment front so that the leading edge of the sample seems to have the highest velocity. This kind of behavior was detected for most of the tests with un-grooved samples. The detachment initiated from the leading edge of the sample for all of the soft rubber samples, and swept across the contact area so that one of the trailing edge corners was the last static contact point.

However, in hard rubber samples at low temperatures, the slip initiated at the trailing edge if the ice cracked during the test. The hard sample also caused errors and interruptions to DIC due to ice cracking and lack of texture and therefore it is not as suitable for this kind of DIC analysis as the soft rubber is.

A data sample collected with Mini-Mu-Road (MMR) is shown in Figure 27. This shows that the friction coefficient is zero before any movement of the rubber sample occurs. When the movement initiates the friction coefficient rises rapidly to high value at first but then drops to lower level where it oscillates around a constant value.

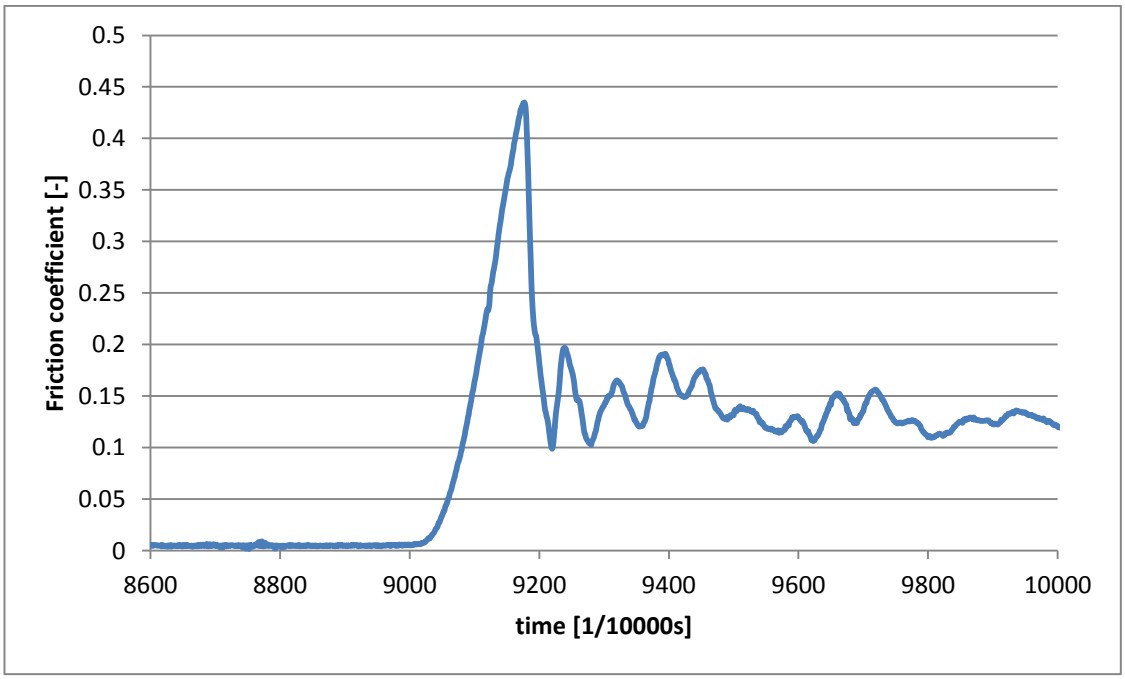

Figure 27 An example of data collected by Mini-Mu-Road.

Figure 28 shows this data put together with the images of digital image correlation (DIC) presented earlier in Figure 27. It seems that the more the detachment front has progressed,

the higher the friction is, until the friction drops rapidly when the whole contact is detached, in other words when the whole rubber sample is moving.

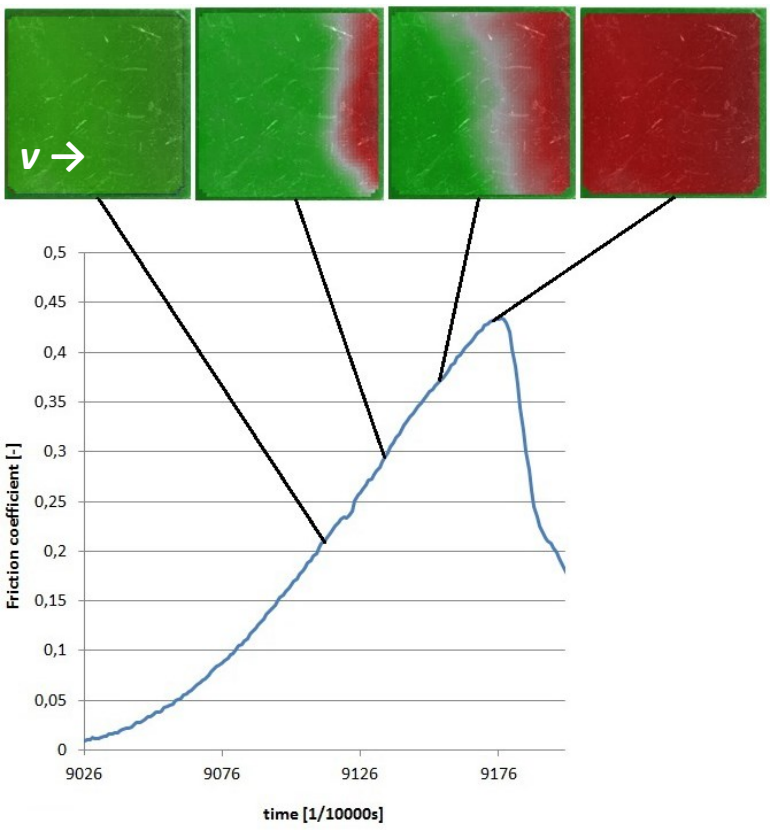

Figure 28 MMR data and DIC data combined. The friction level drops when the whole contact area is detached.

5.2 Raw high-speed video

Long dwell time caused an interesting phenomenon that was recorded with high-speed camera. In the recorded films it could be noticed that a brighter area in the contact area was developing during the detachment. A clear example of this is shown in Figure 29.

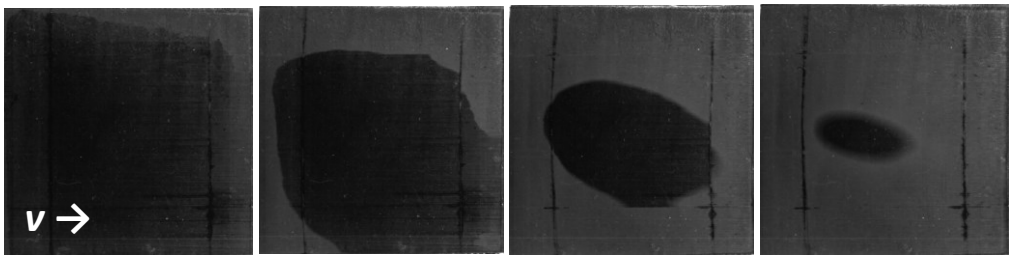

Figure 29 Bright area developing during detachment.

The progress of this brighter area was compared with DIC detachment data to compare if the lighter area was a sign of detachment. In Figure 30 an example is shown of the comparison between the light area of the recorded video and distribution of the contact area velocity. The red values have velocity of 8mm/s or more.

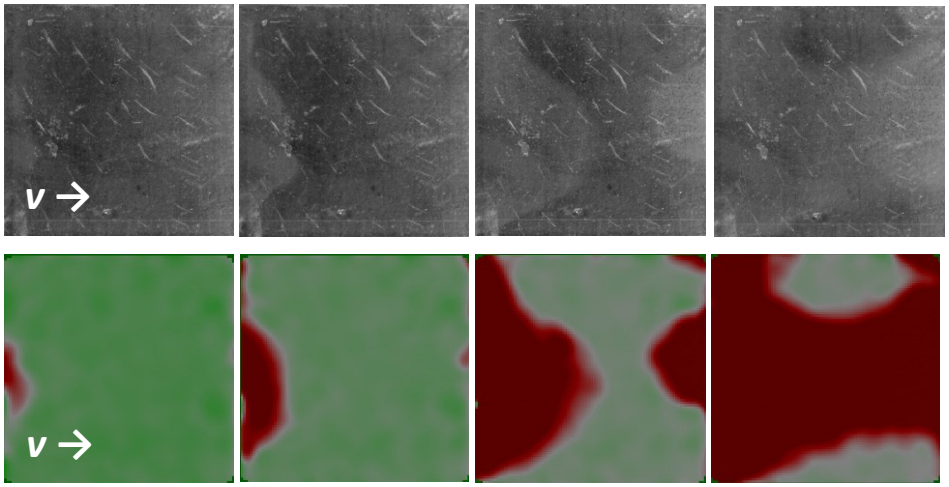

Figure 30 Comparison between bright area and DIC data. The bright area seems to be detached.

It can be clearly noted that the lighter color in the contact represents detachment. The contrast between detached and undetached areas was greater with longer dwell times, and not visible at all for 2s dwell times. The shade difference between the detached area and the undetached area did not change the direction of the velocity calculated by DIC but in cases which had a high contrast between detached and undetached areas the DIC did not yield results.

The darker area has very good connection between the rubber sample and the ice. The long dwell time means that the rubber has a lot of time to adapt to the shape of ice roughness, whereas short dwell times and sliding situations mean that the rubber has little time to adapt. The measurement of the friction levels support this interpretation, since with long dwell time friction coefficients of more than 1 are achieved whereas friction levels of not more than 0,5 are achieved with 2s dwell time, and the dynamic friction coefficient is around 0,3. It could be explained that the detached area is lighter because the contact has more “gaps” between ice and rubber than in the dark area that fills more of the surface roughness. These “gaps” reflect the light differently than the more filled situation. This can be seen from Figure 31.

Figure 31 Rubber sample on surface roughness peaks with short (above) and long dwell times (below). During long dwell the contact area of rubber should grow.

Opportunities made possible by this phenomenon could be that the friction levels could be analyzed by the tone of the color in the contact area or the state of the detachment could be analyzed without DIC software since the detached area can be seen with bare eyes.

The downside of this kind of changes in reflectivity is that DIC may not find a match of subsets because it cannot find corresponding shade of pixels. This can cause errors in the calculation or distort the calculations totally.

5.3 Effect of dwell time

The effect of dwell time on friction between the rubber sample and the ice was studied with MMR, by pressing the rubber sample against ice surface with 800 N force for seven different dwell times ranging from 2s to 600s. This force, which equals to 2,2 bar contact pressure, was selected because it is at the range of passenger car tire pressure. These tests were performed at -5C and -12C with soft and hard rubber.

In Figure 32 the highest values are shown of the friction coefficient measured for each dwell time, different rubber hardness and temperature.

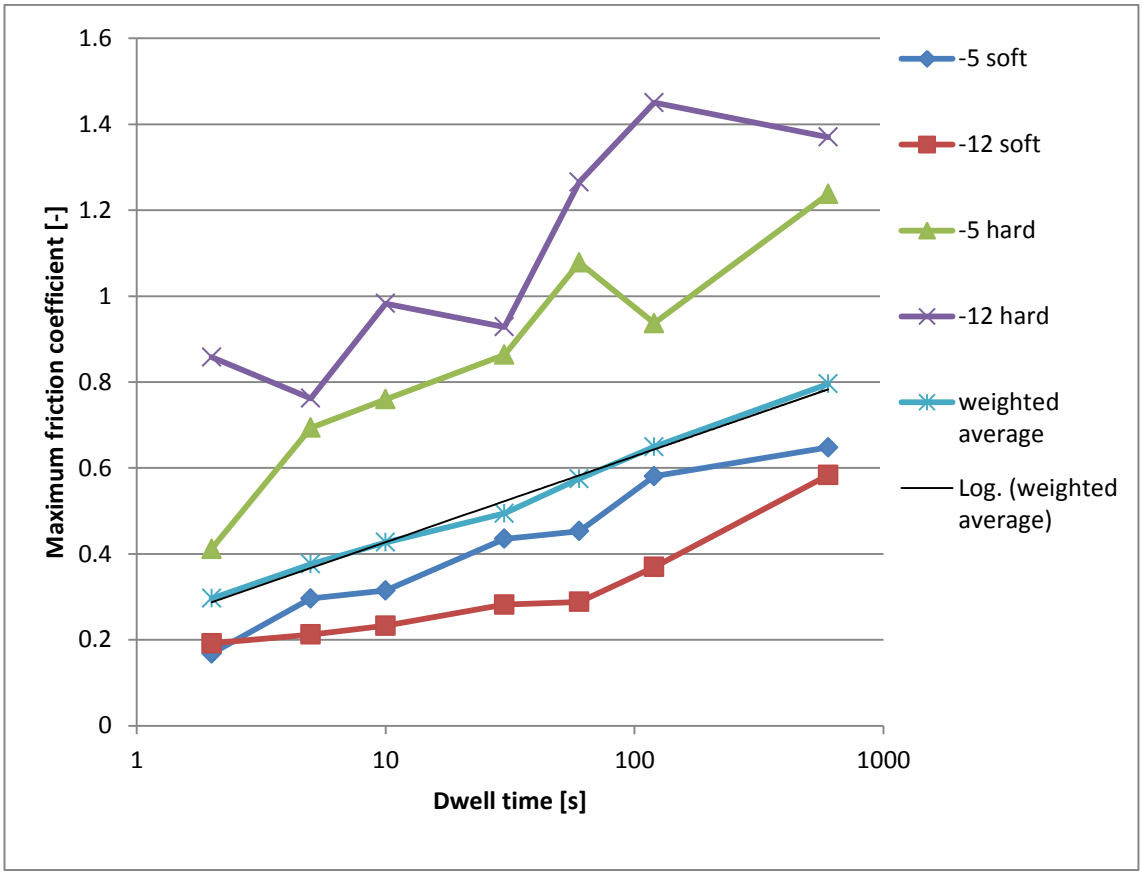

Figure 32 Highest values of friction coefficient for different dwell times, temperatures and rubber samples. Hard rubber gained the highest static friction level.

From the figure it can be seen that the maximum friction coefficient (or static friction coefficient in other words) rises if the dwell time is extended. The weighted average is counted by using weight factors of:

$$a_j = \frac{1}{\frac{1}{n}\sum_{i=1}^{n} \mu_{ij}}$$

where a_j is weight factor for a given combination of rubber and temperature *j*, μ_{ij} is measured friction coefficient for a given dwell time of *i*, and n is the number of measurement points.

The weighted value for a given dwell time is therefore calculated as:

$$\mu_i = \frac{a_1 * \mu_{i1} + a_2 * \mu_{i2} + a_3 * \mu_{i3} + a_4 * \mu_{i4}}{a_1 + a_2 + a_3 + a_4} = \frac{\sum_{j=1}^{n}(\mu_{ij} * a_j)}{\sum_{j=1}^{n} a_j}$$

The weighted average value of the friction coefficient seems to have logarithmic relation to dwell time with function of:

$$\mu(t_d) = 0{,}0869 \ln(t_d) + 0{,}2273$$

where $\mu(t_d)$ is the friction coefficient and t_d is the dwell time. This quantifies the idea of logarithmic dependency of friction and dwell time. The weighted average of friction is almost three times as high with 600s dwell time as it is with 2s dwell time.

It is notable that the fluctuation of the measured friction coefficient for hard rubber is quite high. This could be connected to the detachment mechanism where the contact between rubber and ice is stronger than the contact between ice particles or ice and glass. When the movement is caused by the breaking of the ice rather than detachment of the rubber ice contact, the dwell time won't have the same friction rising effect since the strength of the connection is defined only by the properties of the ice or the properties of the contact between ice and glass plate. This explains the unexpected "drops" in friction coefficient with some elevated dwell times since the strength of the ice at that area is weaker due to imperfections that have formed during the ice preparation or micro cracks that have occurred during the dwell. This ice cracking occurred only with hard rubber so the reason for this could be more uneven pressure distribution in contact, since harder rubber does not adapt to the form of the ice as well as the softer rubber. These high pressure spots may occur in the trailing edge of the rubber sample where the cracking of ice could be found. There was not as much fluctuation with soft sample as with the hard sample. Therefore it seems that the properties of the ice strength vary much more than its frictional properties in this ice preparation method.

The Figure 32 shows clearly the hard rubber gained more static friction than the soft rubber. However, the static friction of soft rubber increased when temperature increased which was not predicted.

Most of the measured videos show a clean detachment that does not visually damage the ice. However, when using long dwell times with hard rubber the friction coefficient raises so high that the contact between rubber and ice is stronger than the contact between ice particles or ice and glass plate. In Figure 33 is shown a test in -12C with hard rubber and dwell time of 60s. The gap between images is 6 ms.

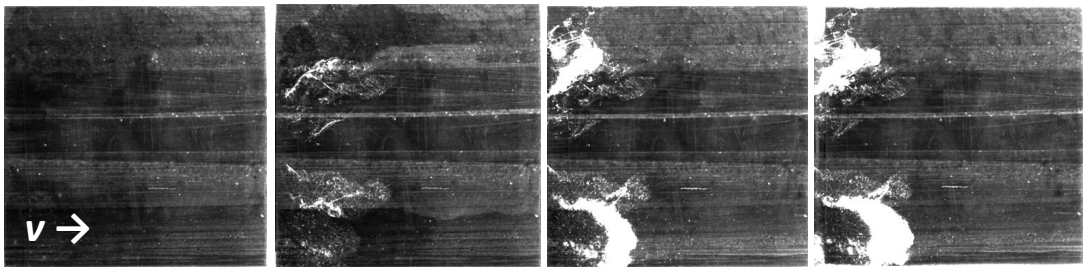

Figure 33 Breaking of the ice in a test with long dwell time. The cracked ice stayed connected to rubber through the whole sliding motion.

In this case the detachment of the rubber sample initiated at the leading edge but the trailing edge never detached from the ice. Instead a half millimeter thick ice layer was cracked off the ice starting to move stuck to the rubber sample. The broken ice was in contact with the rubber sample for the rest of the sliding motion. This can also be seen from Figure 34, where the kinetic friction of dwell times 120 s and 600 s is close to zero, since these dwell times caused ice cracking and sticking to rubber. Removal and sticking of ice can be also seen in the tests with 30 s and 60 s dwell time in smaller scale than with 120 s and 600 s. Their kinetic friction coefficients seem to be a bit lower than the coefficients of the tests with 2 s, 5 s or 10 s dwell times.

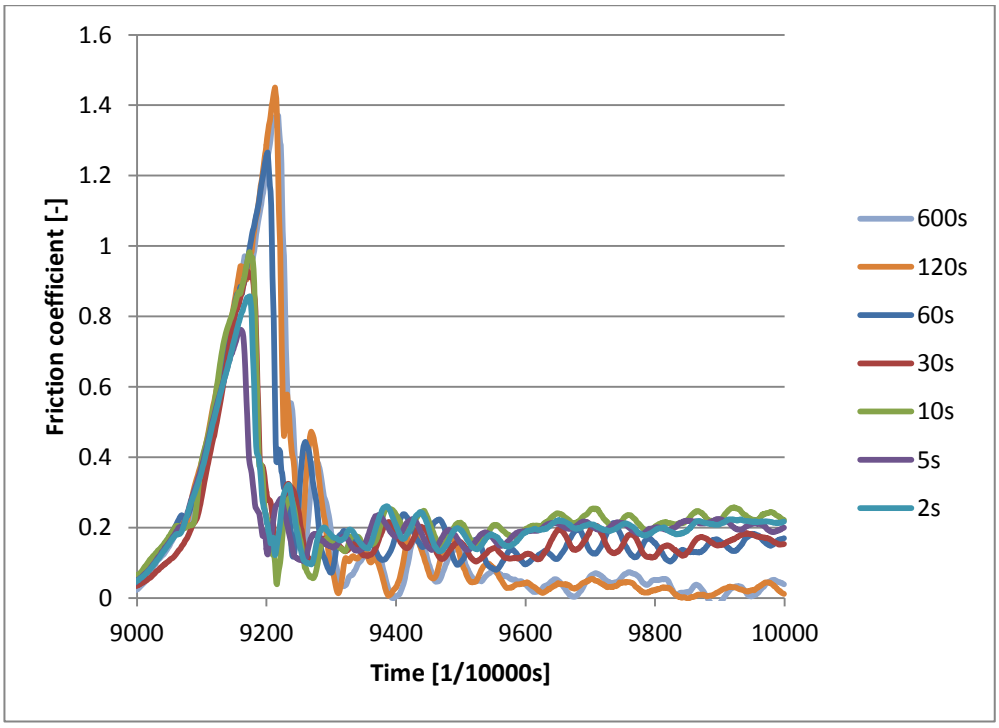

Figure 34 Low kinetic friction of the samples that broke the ice. Dwell times 600s and 120s caused a large crack into the ice, while 60s and 30s caused a small crack.

It is notable that the effect of dwell time does not concern the kinetic friction (if there is not ice cracking during detachment), since the coefficient of kinetic friction of all dwell times is at approximately same level independent from the dwell time as can be seen from Figure 35.

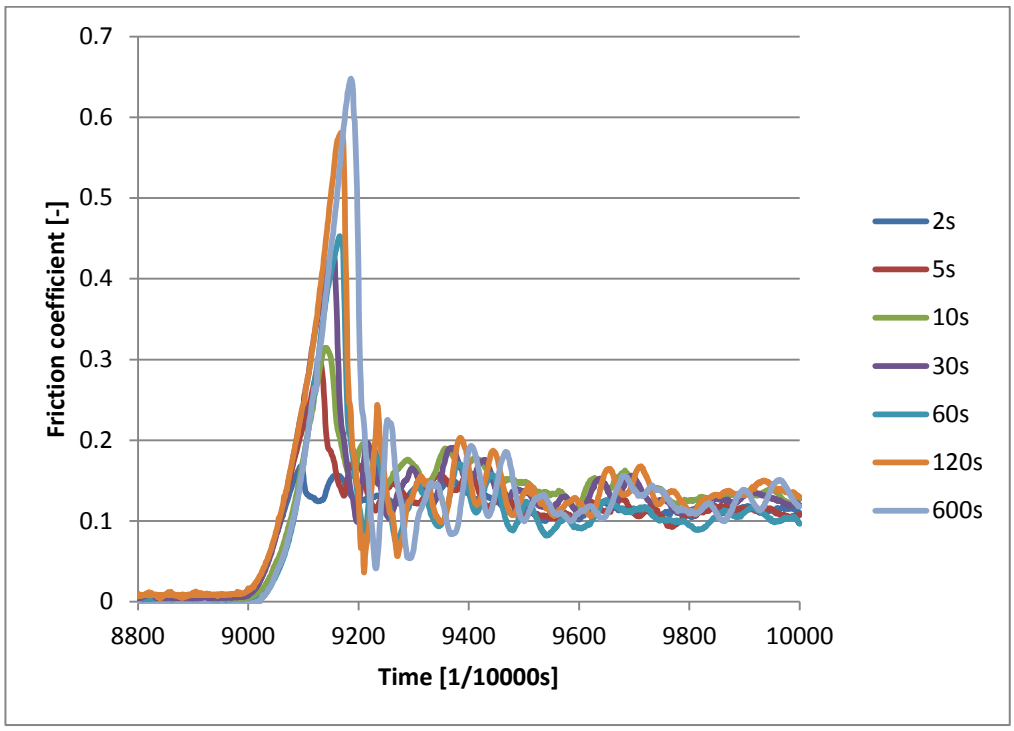

Figure 35 Static and kinetic friction levels for the soft rubber at -5C.

5.4 Precursors

Precursors in friction measurements are small reductions in friction level during the static friction build-un phase. They last only about 1 ms, after which the friction level is rising again. Figure 36 shows an example of the measured data, in which precursors have occurred.

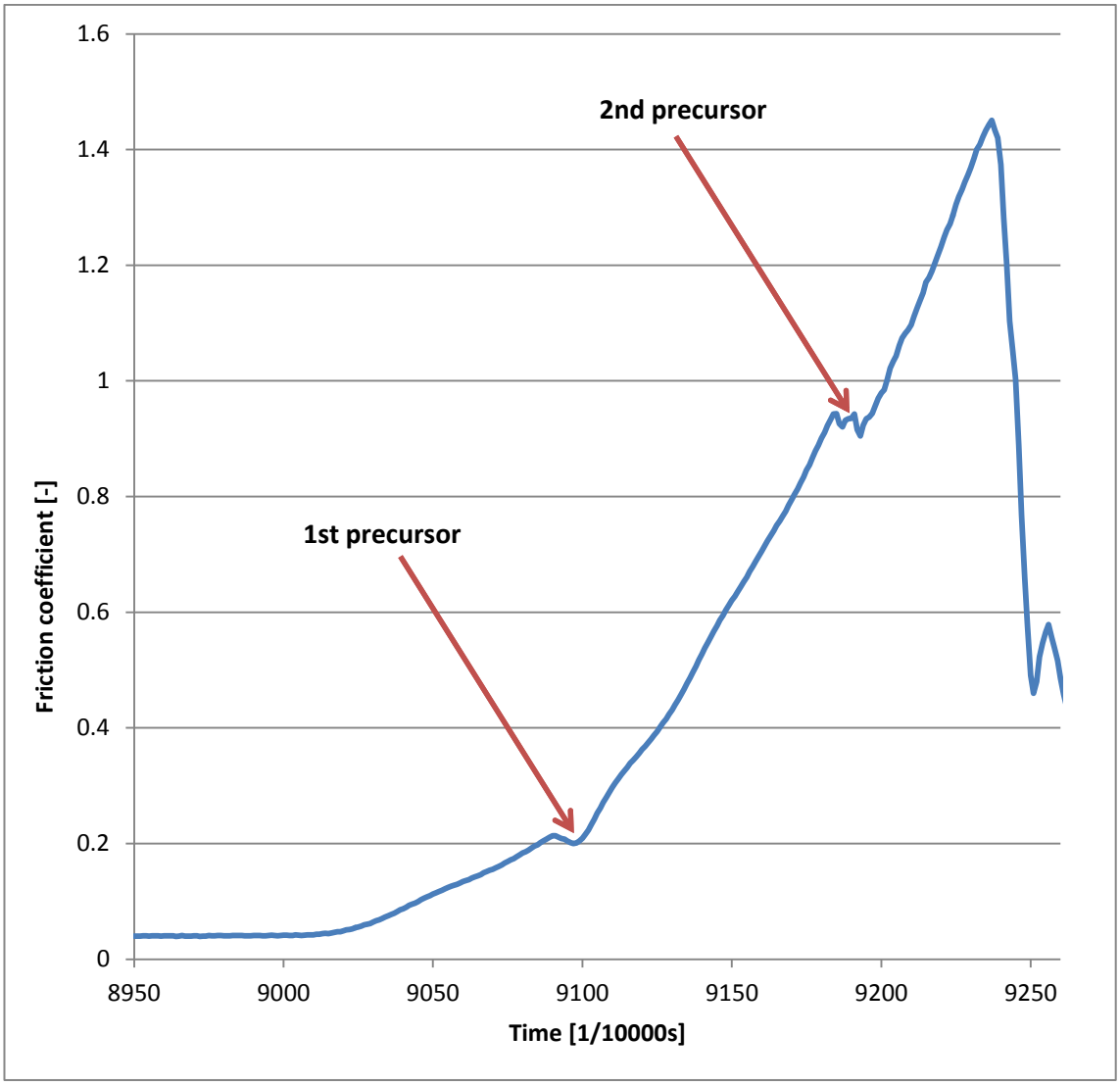

Figure 36 An example of data with precursors.

The friction build-up phase for the hard rubber at -12C with different dwell times is shown in Figure 37. It is clear that there are two separate regions where the precursors occur. The first one is marked with a red circle and second one with a blue circle in the figure.

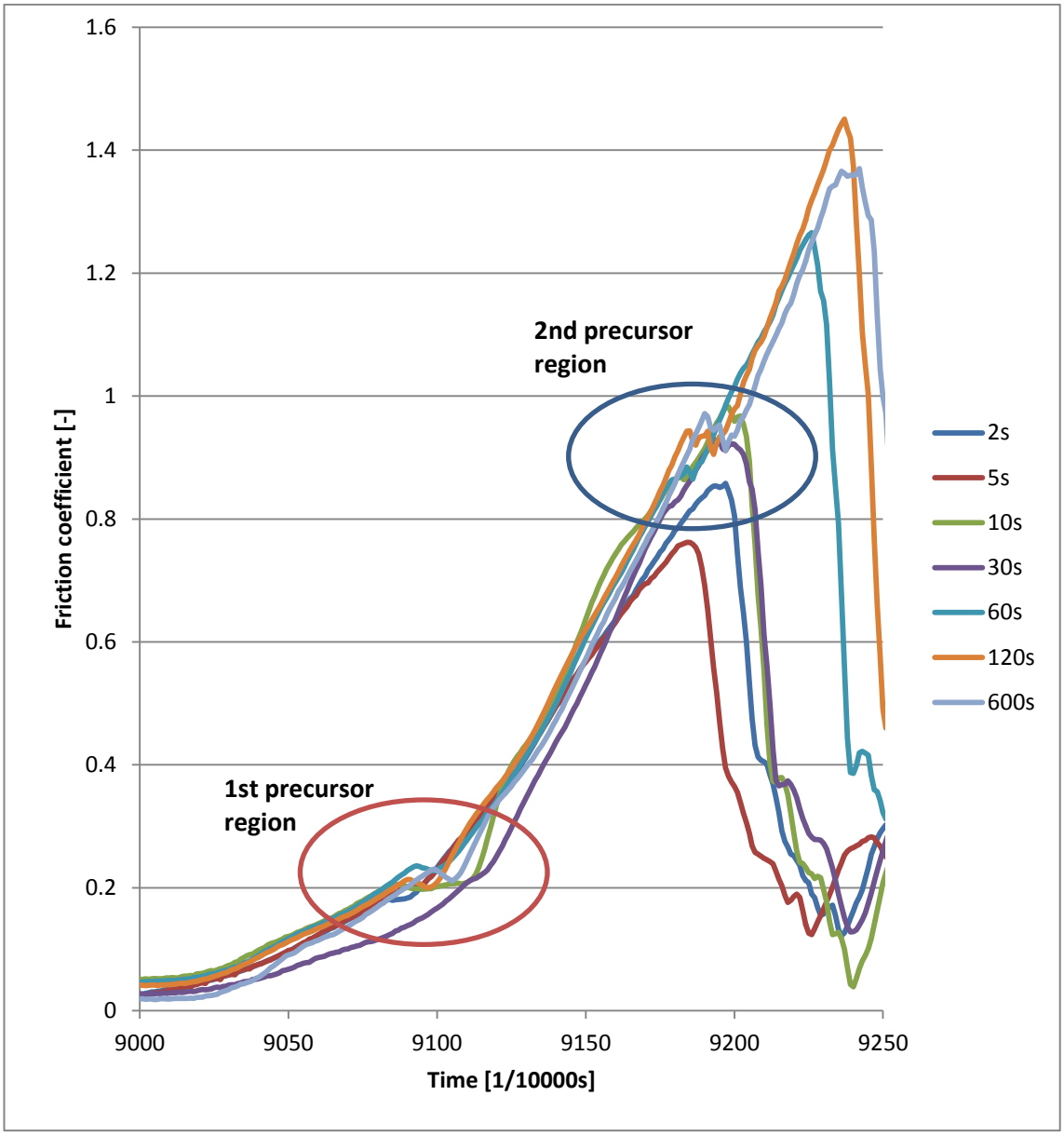

Figure 37 The friction build-up phase for hard rubber in -12C. Two clear regions for precursors can be found.

It should be noticed that for all dwell times for hard rubber either a clear first precursor occurs in data or the development of friction is clearly slowed down. Also notable is that the first precursors occur at surprisingly same friction level, since the range for all first precursors is from $\mu = 0{,}18$ to $\mu = 0{,}24$. A clear second precursors occur only if the friction coefficient rises above 0,85 which is not the case for 2s and 5s dwell times. For longer dwell times a clear second precursor is notable. The second precursor has a clear region to occur which is between $\mu = 0{,}85$ and $\mu = 0{,}95$.

The results for hard rubber in -5C can be seen from Figure 38. It shows that the region for the first precursor is approximately the same as it is at colder temperature.

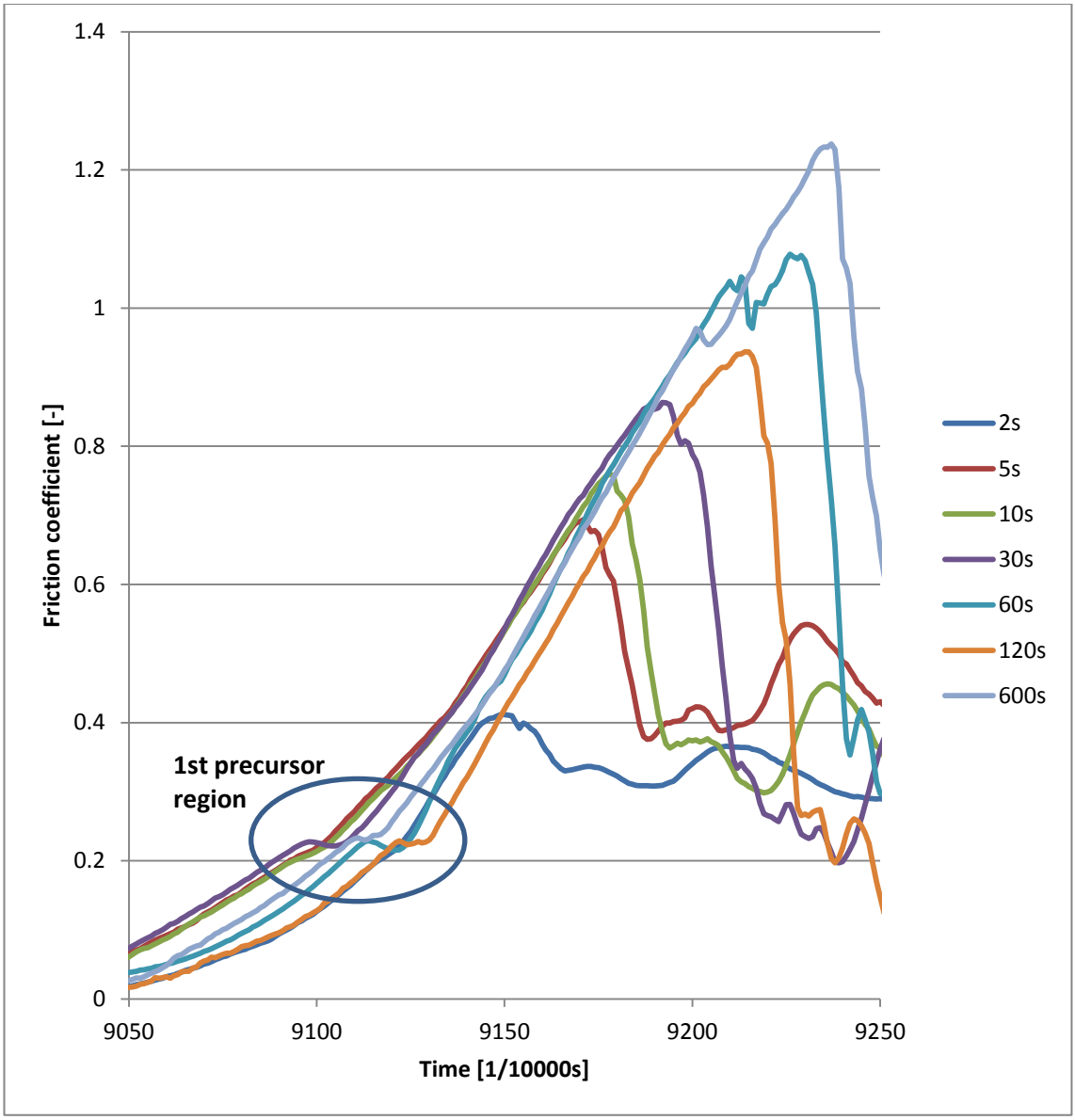

Figure 38 The friction build-up phase of the hard rubber in -5C. The friction level of the first precursor is surprisingly same for all dwell times.

Only dwell times of 60 s and 600 s resulted a second precursor, because these were the only dwell times that produced clearly over 0,9 friction coefficient. The dwell time of 120s produced friction coefficient in this region, but since its level of friction is much lower than the friction of 60s dwell time there may have been an unexpected phenomenon that overplayed the effect of dwell time. This could be the reason for no visible second precursor. Figure 39 shows the zoomed view of the first precursor region.

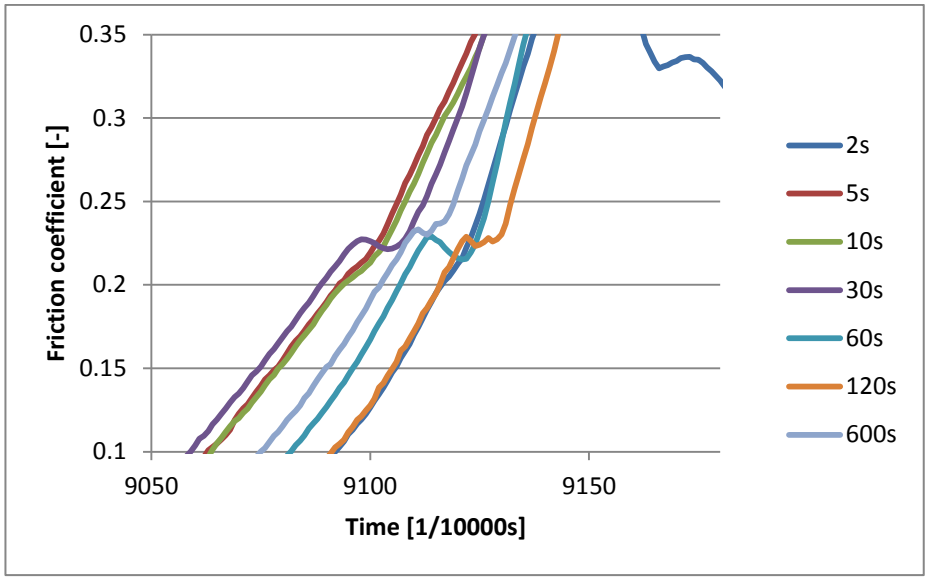

Figure 39 Zoomed view of the precursors.

There are no clear precursors for small dwell times (2s, 5s and 10s) but a reduction in friction development can still be seen in the same first precursor region.

The results of the tests with soft rubber sample at -12C are shown in Figure 40. There are no clear precursors at dwell times under 600s. In some cases a slight reduction in friction build-up slope can be found near μ = 0,2, but clear precursor cannot be found. The only clear precursor can be found with 600s dwell time at μ = 0,48.

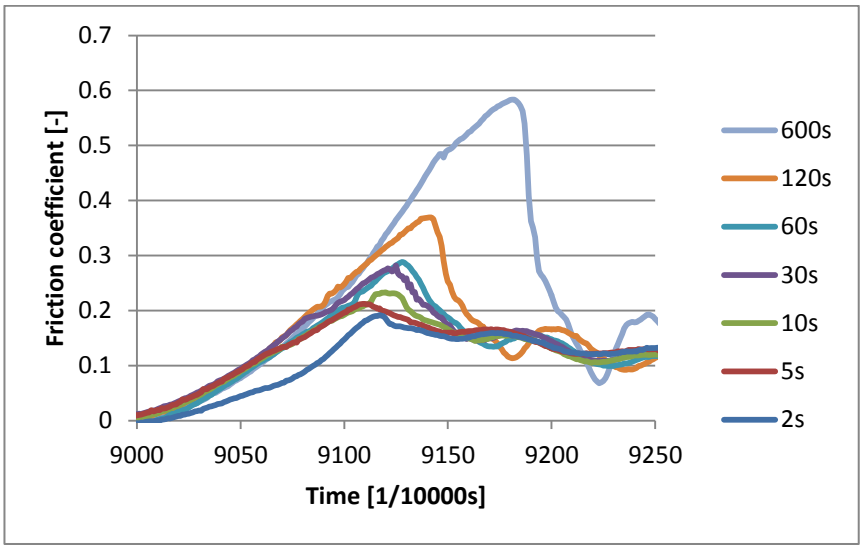

Figure 40 friction build-up phase of soft rubber in -12C. There are no clear precursors.

The results of the soft rubber at -5C can be seen from Figure 41. In this case also the only clear precursors can be found with 600s dwell time but at lower friction level at μ = 0,26.

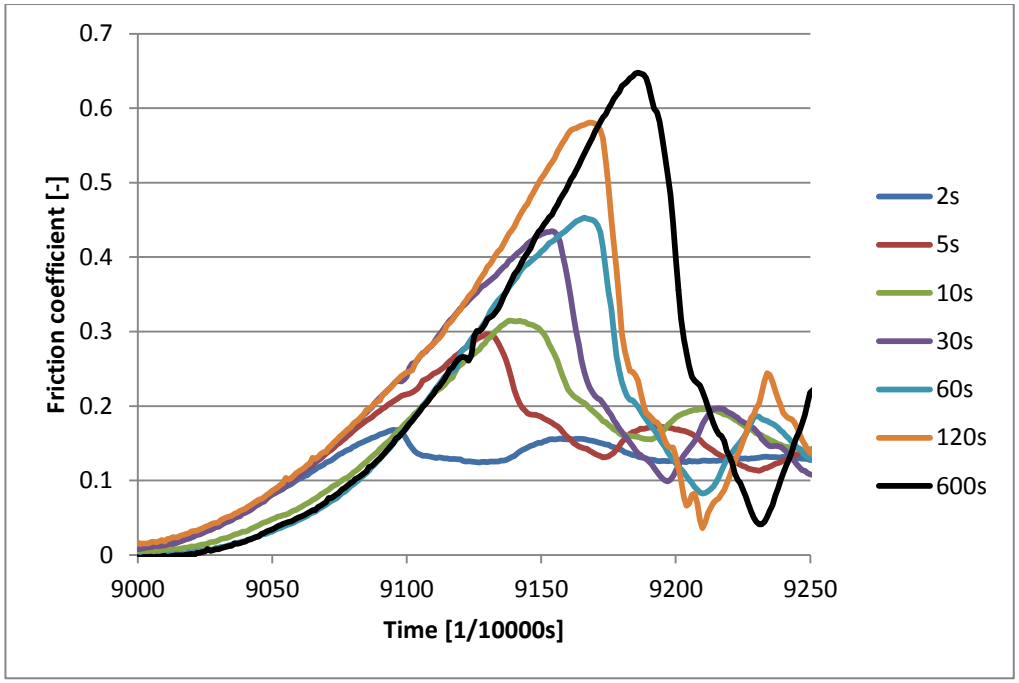

Figure 41 The friction build-up phase of soft rubber in -5C. Only one clear precursor was found.

This differs from the precursor position of the soft rubber at lower temperature which is different to behavior of the hard rubber. The hard rubber had a clear region for the precursors that was the same for different temperatures. Either the soft rubber causes weaker precursors or the friction level, where the precursors occur, is higher. The soft rubber may not be as prone to precursors as the hard rubber is.

In the Figure 42 is shown high-speed camera data combined to friction data at first precursor of 5s dwell time with hard rubber in cold temperature.

It seems that the first precursor occurs in data when the first visual signs of detachment appear. If there were precursor or precursors in measured data, the first precursor occurred at the same time with the first visual signs of the detachment. However, even if the precursors were clearly combined with the initiation of the detachment for hard rubber compound, there were no precursors when the detachment initiated in the soft rubber.

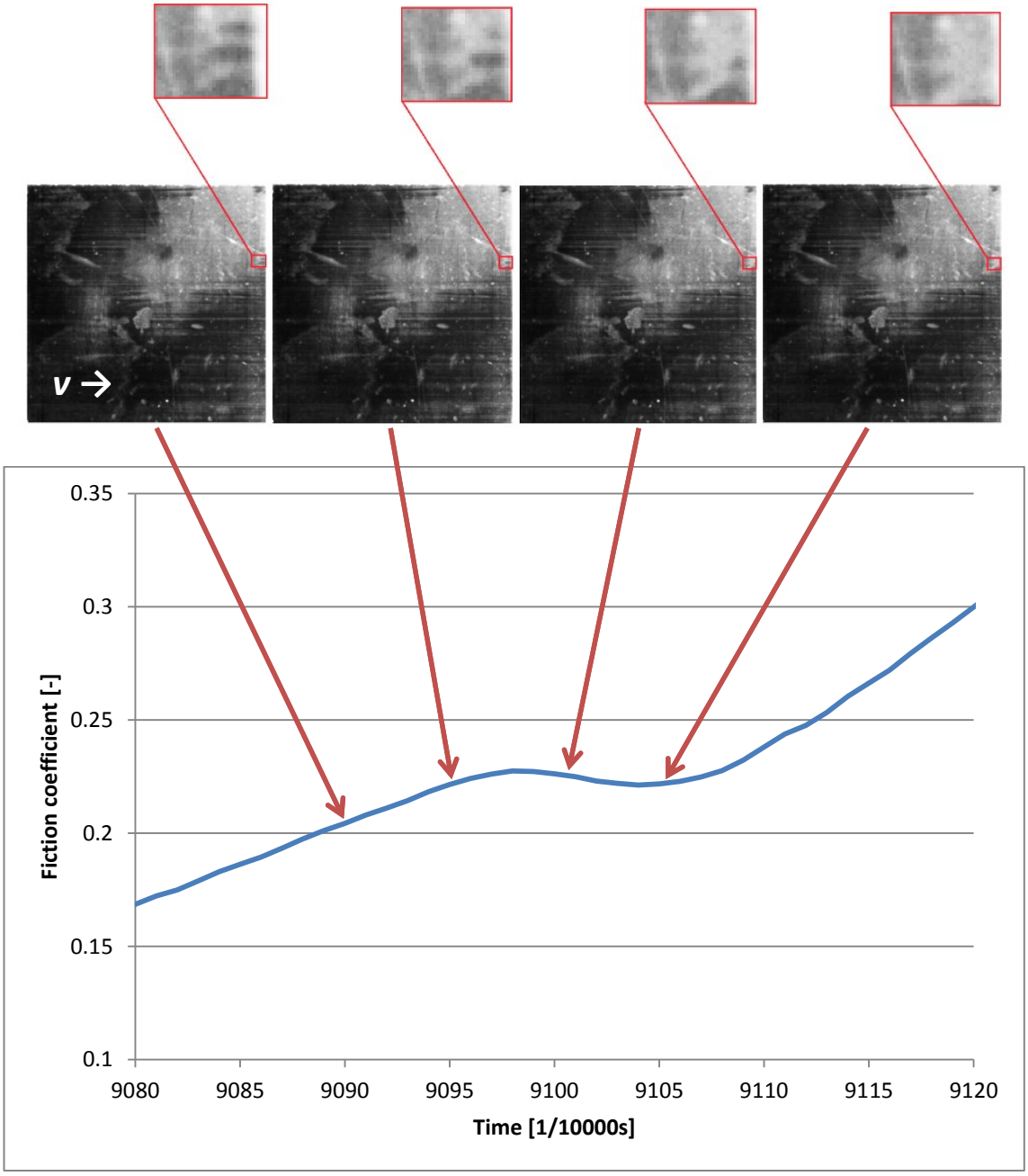

Figure 42 Friction data combined with high-speed camera data at first precursor. The first detachment area is zoomed in red box. No DIC could be made since the hard rubber lacked texture and cracked the ice.

The notable thing about the second precursor is that it occurs only if the friction coefficient rises close to μ = 0,9. At the tests that gained high friction and a second precursor occurred in the data, the ice was cracked during the initiation of the sliding motion. This is because the frictional force was high enough to create a shear tension to the ice that was greater than the shear strength of the ice. The contact of ice and rubber was so strong that small ice plates (with areas from 10mm x 10mm to 30mm x 60mm) were stuck to the rubber sample and had

to be removed from the sample between the tests. These ice plates were mostly a result of breaking of ice-ice contact but on some cases the small ice plate detached from the glass.

There were no second precursors with softer rubber compound. The low friction levels may be the reason for this since the stress of the ice was not as high as for the harder rubber that damaged the ice.

In Figure 43 is shown the friction data of the second precursor combined with the high-speed camera data at -12C and with 60s dwell time for the hard rubber.

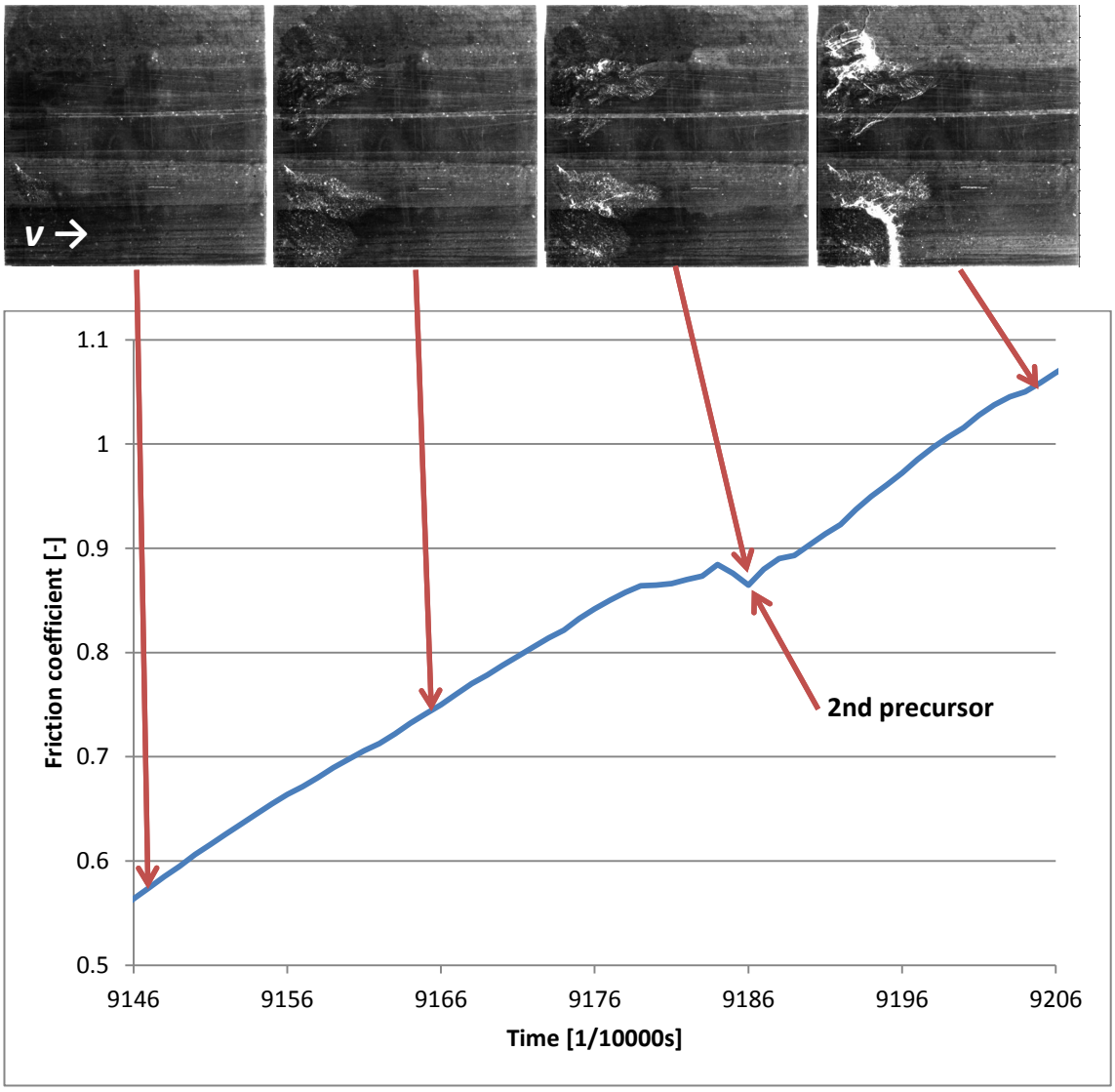

Figure 43 The friction data combined with the high-speed camera data at the second precursor. The second precursor occurs near the initiation of the cracking of the ice.

It is possible to see from second image frame that the ice has actually started developing cracks before the second precursor. For the rest of the measurements the first visual cracks could have been seen at the friction coefficient level that differed ±0,1 from second precursor. Sometimes the visual cracks were noticed after the second precursor and sometimes before it. It should be noted that small cracks are easier to notice on the areas that are detached and it is possible that cracks have initiated always before the second precursor. However, all of the tests, in which second precursor occurred, had clearly overloaded the ice and therefore the second precursor seems to be a consequence of the ice breaking.

5.6 Contact pressure

The effect of the contact pressure in friction was tested with the soft rubber sample and three different normal loads: 600N, 800N and 1000N, which correspond to contact pressures of 1,67 bar, 2,22 bar and 2,78 bar. These loads were selected with dwell times of 2s and 60s to see if the changes in the contact pressure result notable differences in friction coefficient or in the detachment pattern of the rubber. The tests were done in the same ice plate within one hour time to minimize the effect of the ice changes over the time. The frictional data collected with MMR is shown in Figure 44.

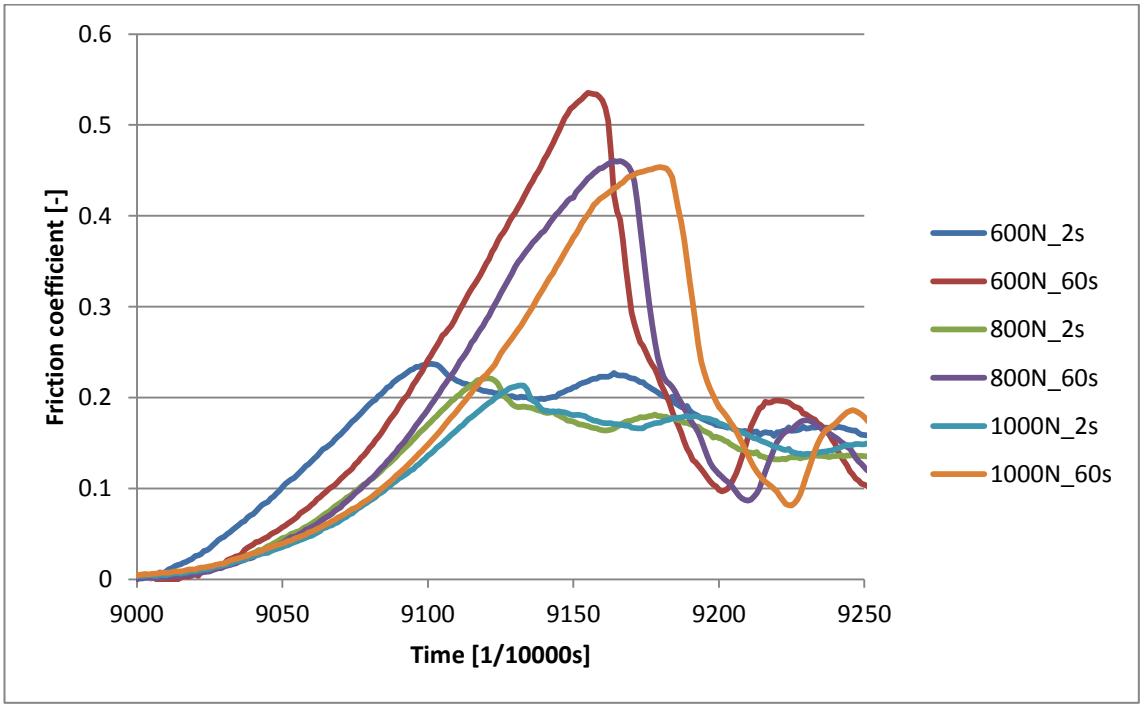

Figure 44 The results of the contact pressure test. Increasing the normal load decreases the friction coefficient.

It can be clearly noted that the higher the contact pressure is the lower the maximum static friction coefficient is. Both tests with 1000N loading force results the lowest static friction of the specific dwell times, whereas the test made with 600N resulted the highest friction coefficients of the specific dwell times.

The reduction in the friction coefficient at higher loads can be explained by that the contact area of the rubber does not grow linearly with the added load. For most solids the contact area grows as a linear function of the normal load, whereas rubber adapt to the counter surface well even with small normal loads and therefore additional load does not increase the contact area linearly.

In Figure 45 are shown the detachment patterns of the 2s dwell time with all three loads. It seems that the detachment patterns are similar, since all detachments initiated at the middle part of the leading edge. When the leading edge was fully detached the front travelled perpendicular towards the trailing edge. The lowest corner was the last static contact point before the whole contact area was detached.

The time between the first sight of detachment to the detachment of the whole contact area took 7,6 ms for 600N; 5,4 ms for 800N and 5,8 ms for 1000N. The development of the detachment for the 600N load seems to be slower that the rest at the last part of the detachment. The detachment went fast from the middle of the contact area to trailing edge for loads of 800N and 1000N, whereas this phase was much slower for 600N. This might be just a random error in measurements, but it showed that the development speed may vary depending of the load. It should be also noted that the test with 600N load got significantly higher friction coefficient than with loads of 800N and 1000N, so the development speed may be connected to friction coefficient.

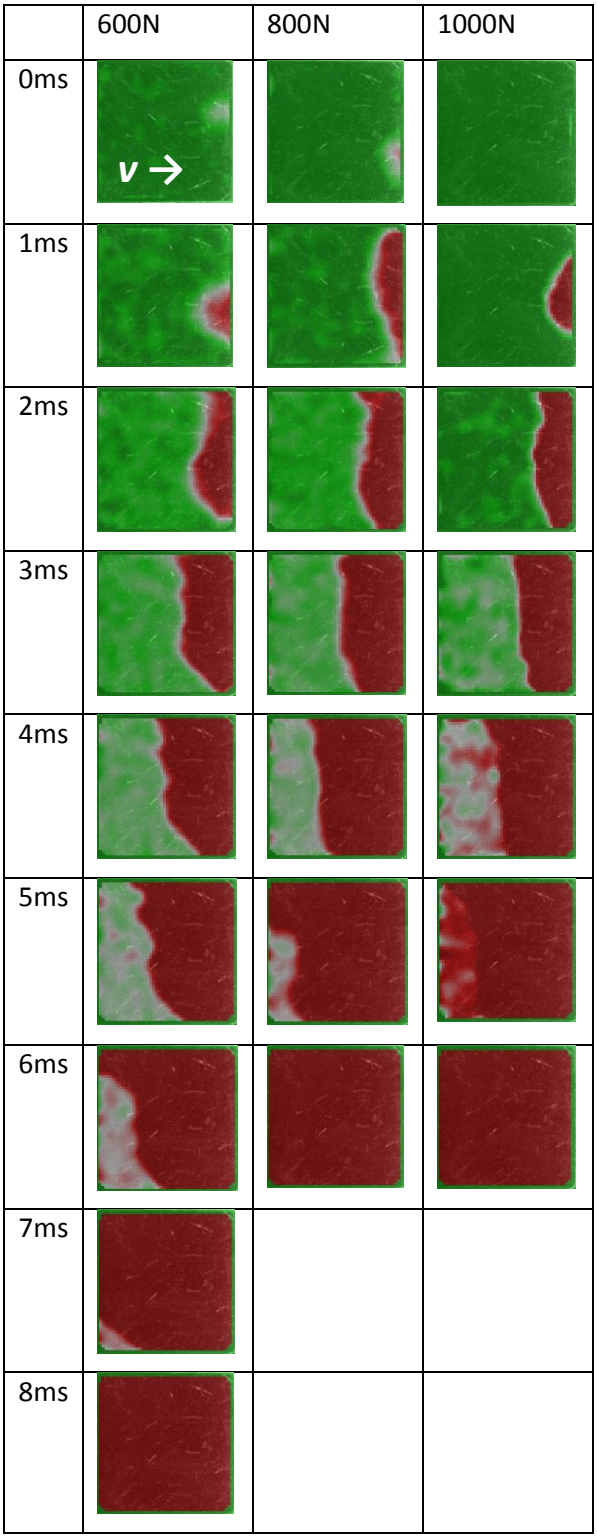

Figure 45 Detachment patterns of 2s dwell time. The slip propagation seems to have the same detachment pattern independent of normal load. With 600N load the contact lasted in the longest and gained the highest friction coefficient.

Figure 46 shows the detachment front development of the different loading conditions under 60s dwell time. The detachment pattern seems to be the same as for the 2s dwell time: The leading edge is first detached from the middle part of the sample, which is followed by the leading edge detachment, and finally the front travelling across the surface. The lowest trailing edge corner stayed in contact for longest.

Time period from the first sign of detachment to detachment of the whole contact area is 3,8ms for 1000N load; 4,8ms for 800N and 6,6ms for 600N. The detachment time is longer for lower pressure as it was for 2s dwell time.

It seems that increasing the dwell time or the contact pressure cause a faster detachment. The faster detachment front developing might be a result from greater forces acting in the rubber. The shear tension and the normal tension of rubber are higher with higher load, and greater force is accelerating the detached rubber, which might lead to faster detachment front progress.

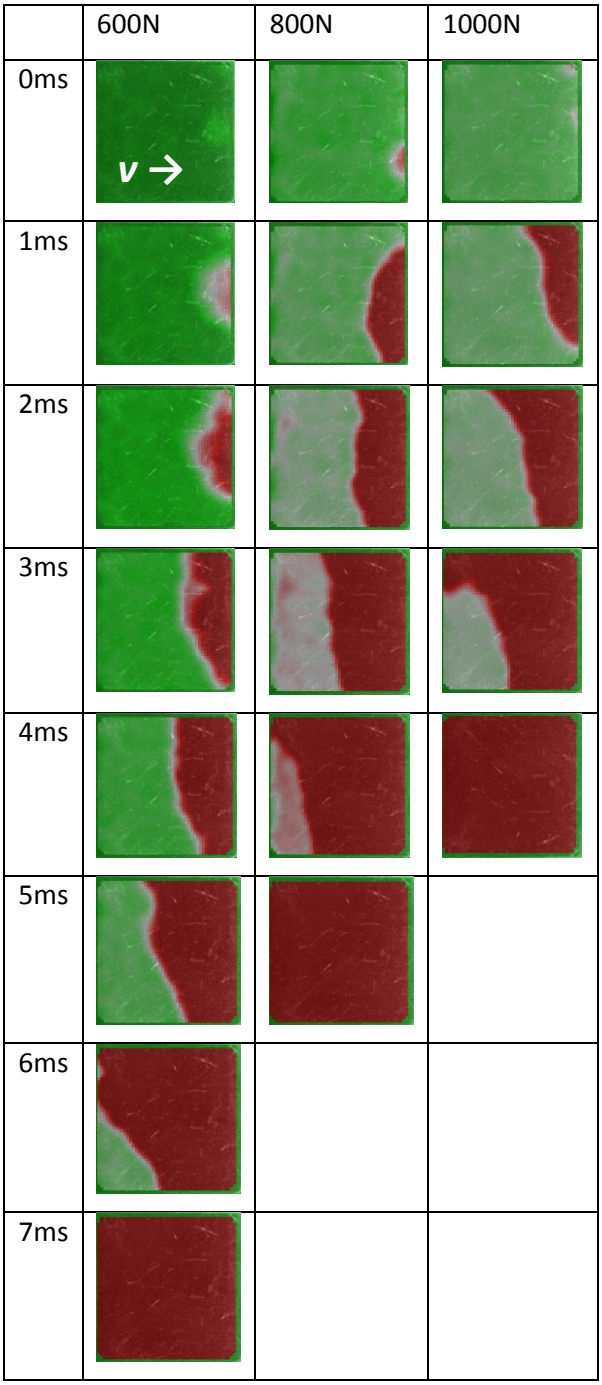

Figure 46 The detachment patterns of 60s dwell time. The slip propagation seems to have the same form independent of the normal load. With 600N load the contact lasted in the longest and gained the highest friction coefficient.

5.7 Rubber texturing

5.7.1 Results

Texturing of the rubber sample was carried out to study the possibility to redirect or cut the detachment front progress. The detachment fronts of smooth rubber samples typically initiated at a point at leading edge and developed fast along the leading edge before sweeping over the contact area. The last contact point was typically either at side edge or at trailing edge.

The tests were done with three different soft rubber samples. The un-grooved sample was the same as in the soft sample in previous tests, small grooved sample had 1mm depth grooves made by a blade so groove width was practically zero. The large grooved sample had grooves with 1mm depth and 1mm width.

The initiation of the sliding motion was recorded with high-speed camera and the shear force and normal load were measured by MMR. Tests were done with 2s, 10s and 60s dwell times. The friction data of the tests can be seen in Figure 47, Figure 48 and Figure 49.

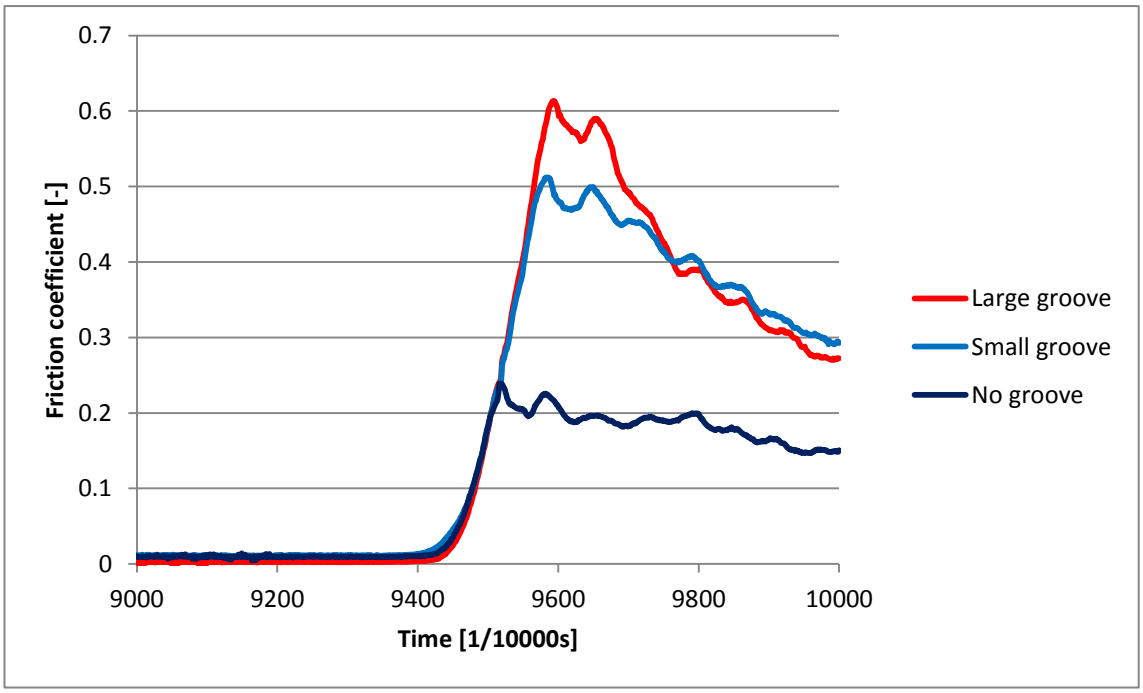

Figure 47 Comparison between grooved and un-grooved samples with 2s dwell time.

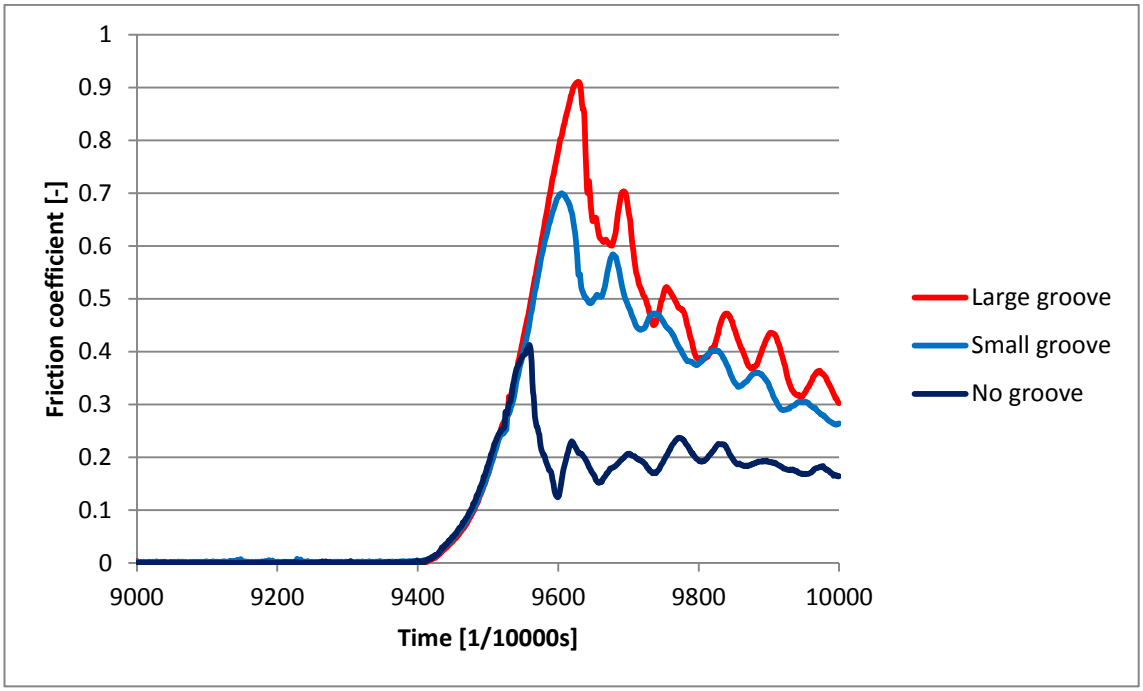

Figure 48 Comparison between grooved and un-grooved samples with 10s dwell time.

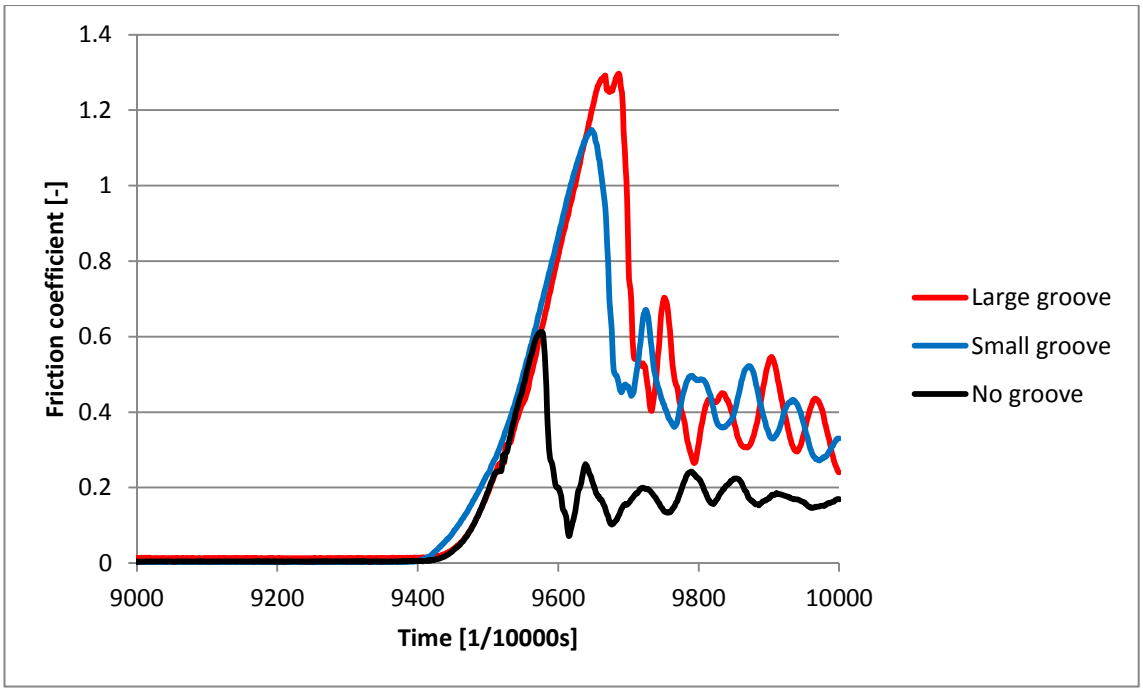

Figure 49 Comparison between grooved and un-grooved samples with 60s dwell time. Grooving seems to increase friction.

It can be seen that the grooved samples produced significantly more friction than the un-grooved sample.

It was notable that with 60s dwell time the friction got higher than in the tests with the hard rubber, in which the ice was damaged. However, the ice was not visually damaged and no ice was stuck to rubber sample. This might be because of the better properties of the ice that was prepared for the tests or more even load distribution on ice because of softer material.

The detachment front behavior of the samples can be seen in Figure 50. It can be noted that the detachment of the smooth sample began at leading edge just as in most of the cases. The upper side edge detached next and the leading and the trailing edges after that. Then the detachment front swept through the rest of the contact area and the detachment ended at the lower side edge.

The small-grooved sample detached first from the upper leading edge corner just as the smooth sample. However the upper vertical groove seemed to hold the progress of the detachment front. The same happened on every groove and it resulted that the detachment front ended in the middle of the sample.

The same happened with the large groove sample but the effect was even more significant. The grooves in the upper leading edge seem to stop the detachment of the leading edge so the center of the leading edge and the upper side edge are in contact even when the trailing edge and lower side edges have detached. The last detached point is in the center as it was with smaller grooves.

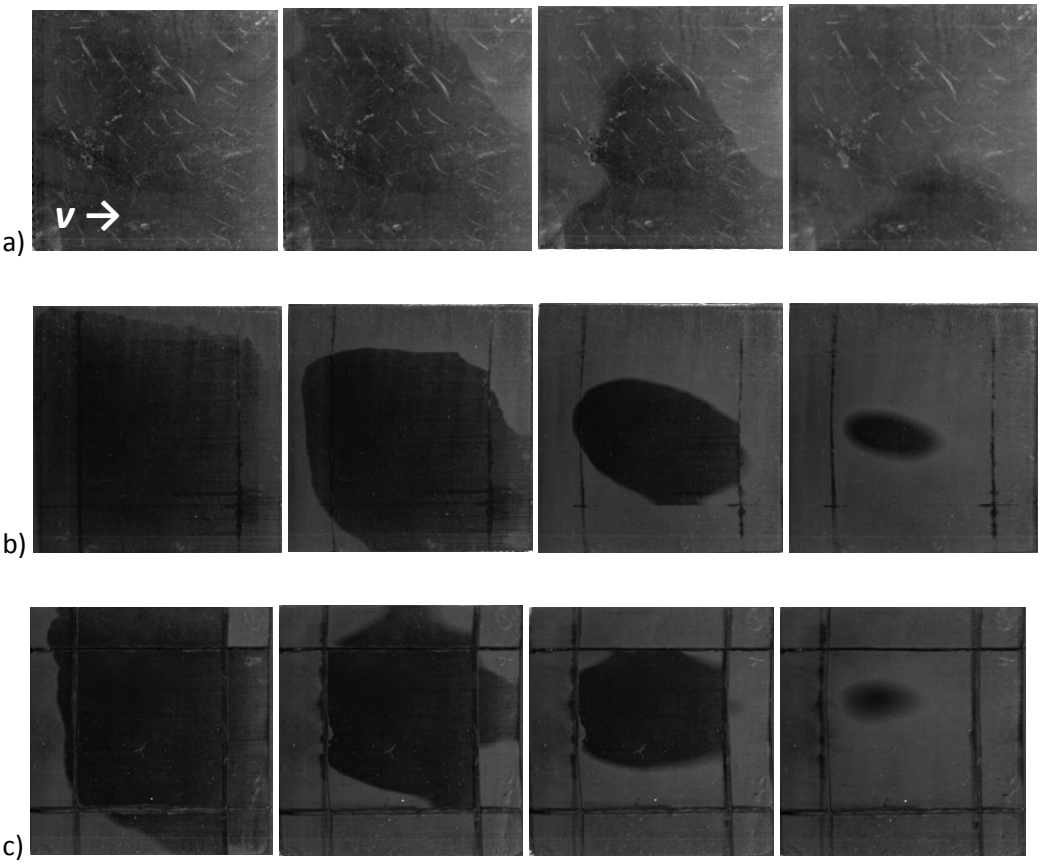

Figure 50 The detachment front development of sample with a) no grooves b) small grooves and c) large grooves

The result means that it seems to be possible to modify the detachment front development by grooving the sample. On the other hand it should be noticed that grooving affects the initial shear forces that are caused by pressing the rubber sample against the ice so that may also be the cause for the increased friction levels and the different detachment front progress.

5.7.1 FEM analysis of the effect of grooves

Because the rubber texturing increased the friction significantly, a finite element method analysis was made to analyze how the grooves affect the surface pressure and initial shear forces of the samples.

Models for all three samples were made with Solid Mechanics physics of Comsol Multiphysics. Rubber was modeled with a two-parameter Mooney-Rivlin material model, using values 0,37 MPa for C_{10} and 0,11 MPa for C_{01}. The initial bulk modulus was 1000 MPa and the density 1100 kg/m^3. The counter surface was modeled as fixed and the material was structural steel. The

friction coefficient was 0,2 for low friction analysis and 1 for high friction analysis. Analyses were stationary.

Mesh for both blocks had the form of free tetrahedral and the size of mesh was extra fine. The constructed mesh is shown in Figure 51. The normal load was applied by prescribed displacement of 0,2mm of upper surface of rubber block. This correlates to ~1000N normal load.

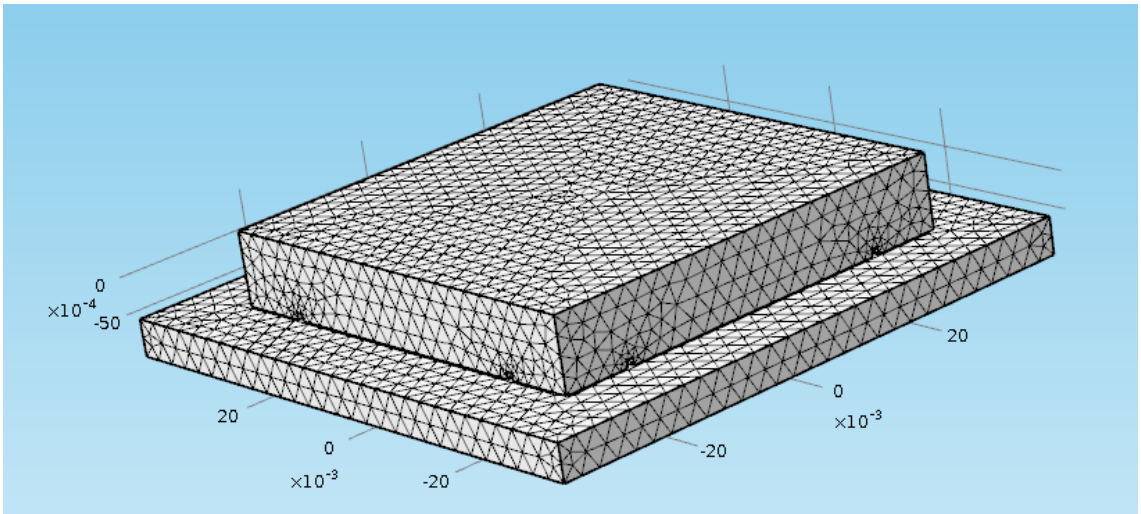

Figure 51 The mesh of the FEM model. The mesh is smaller near the grooves.

In Figure 52 and Figure 53 are shown the surface pressure distribution and the initial shear distribution of un-grooved and grooved samples. The counter surface was rigid and the friction coefficient between surface and rubber was 0,2 and 1, respectively.

It can be noted that the grooves do not affect significantly the contact pressure distribution and at low friction level the initial shear is quite similar in all of the samples. However, the initial shear was altered in high friction situation as the inner part close to grooves and edges seems to be under the most initial shear. Also the peak shear was higher in grooved samples than in un-grooved sample. The grooves relieved shear on the side which was further from the center of the sample and increases shear on the inner side of grooves.

At high friction level the initial shear is high at the center of the edges and decreases towards the center of the smooth sample. The grooved samples have higher initial shear close to edges, but the shear is dropped quickly near the groove. On the other side of the groove the initial

shear increases again to a high level and decreases towards the center of the sample. This makes a square of low initial shear just outside groove. The high initial shear of edges and low shear square might be the reason why the last contact point was located in the center of the sample. The edges detach easily but the low shear square does not, which leads to situation where all of the edges have detached but the low shear square is still on contact.

It should be noted that this FEM analysis did not consider the shear force that is applied to sample at initiation of the sliding.

Initial shear **Contact pressure**

a)

b)

c)

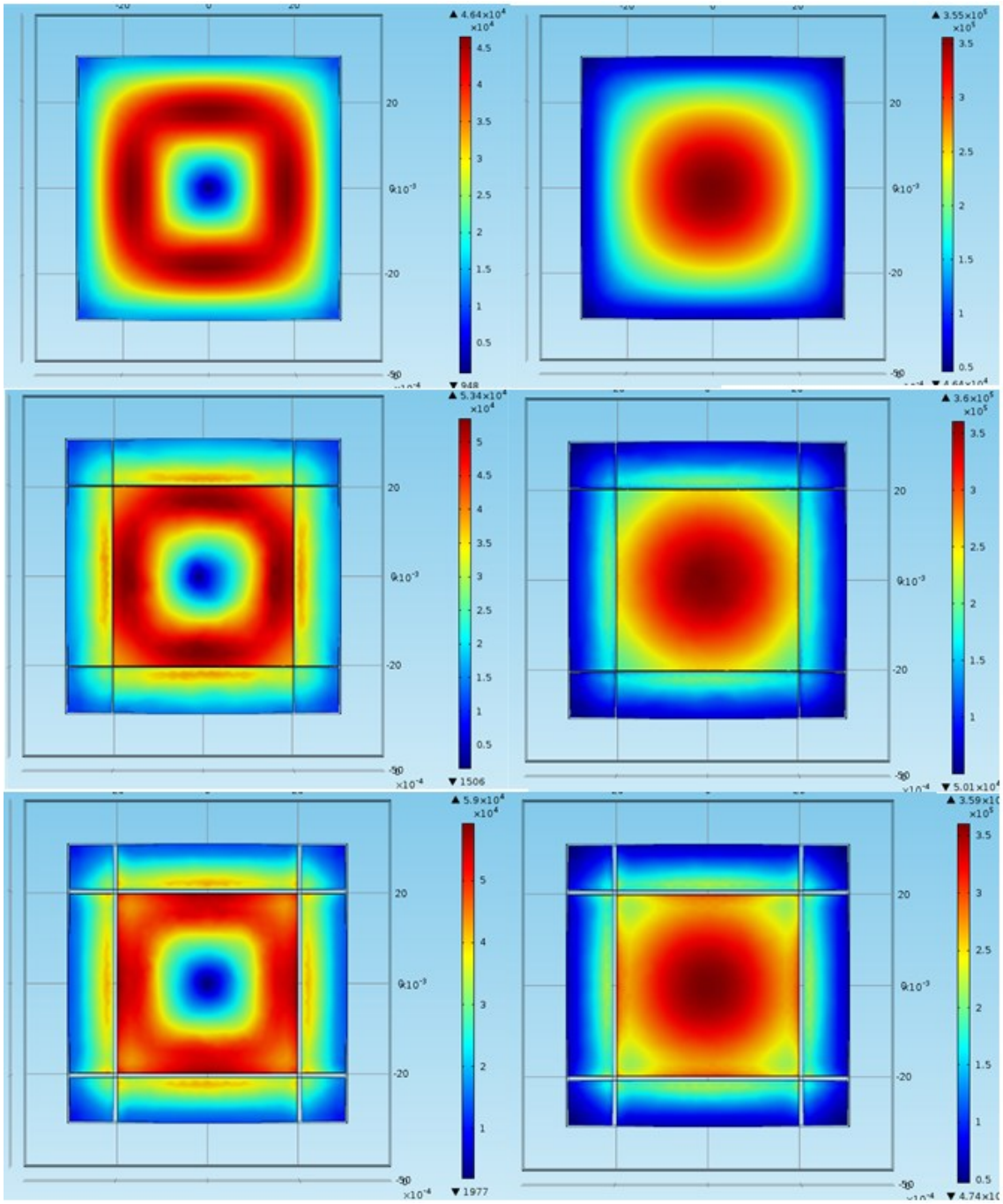

Figure 52 μ = 0,2. The initial shear distribution (left) and the surface pressure (right) of a) un-grooved sample, b) sample with small grooves and c) sample with large grooves. There is no great difference between the samples at this friction level.

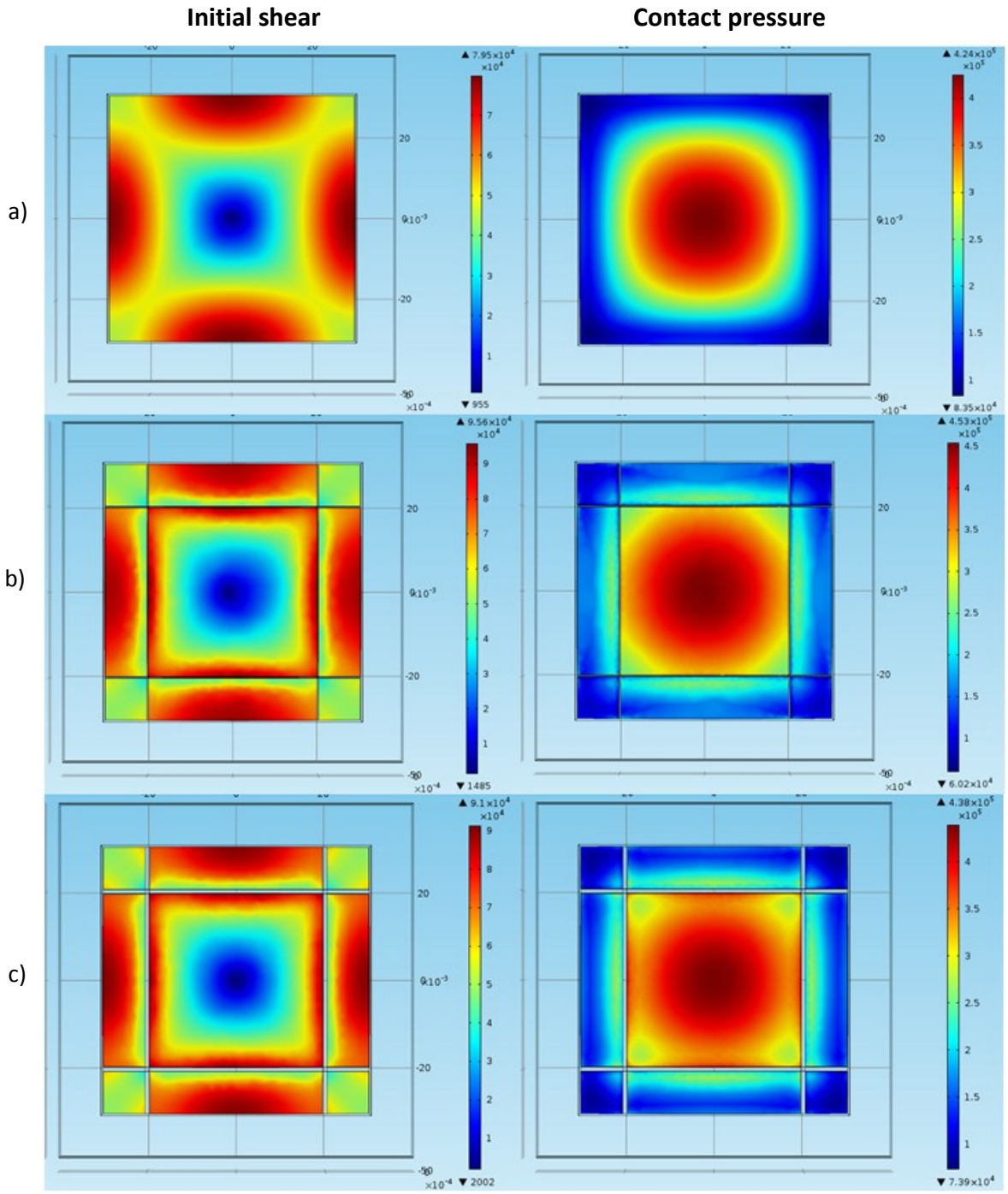

Figure 53 μ = 1. The initial shear distribution (left) and the surface pressure (right) of a) un-grooved sample, b) sample with small grooves and c) sample with large grooves. A clear difference can be noticed on the initial shear distribution between smooth and grooved samples. A "low shear square" and higher peak shear can be found from the grooved samples.

5.8 High-speed camera light heat effect on measurements

a high-speed camera requires good lighting conditions when recording with high frame rate. The shutter speed that is used is the same as the recording frequency so the shutter time is 1/5000s which is really small period of time for the sensor of the camera, and therefore a lot of light power is required. The light source must be powered with stable direct current transformer since all fast deviations in the lighting are shown in recorded video.

Stable lighting is achieved in these measurements by high power halogen lamps which generate a great amount of heat during operation. They are manually switched on before the sliding motion initiates. Their on-time effect to friction levels were tested to decide which on-time would be the best compromise between the error in measuring and the usability of the measuring equipment.

The test were made on virgin ice tracks so that the ice was let to cool down at least two minutes after previous test and the new test line was more than 300mm away from last measured track to minimize the effect of the heat transformation. The dwell time for the test was 2s. The result can be seen in Figure 54. The maximum friction coefficients are plotted as a function of on-time of lights in Figure 55.

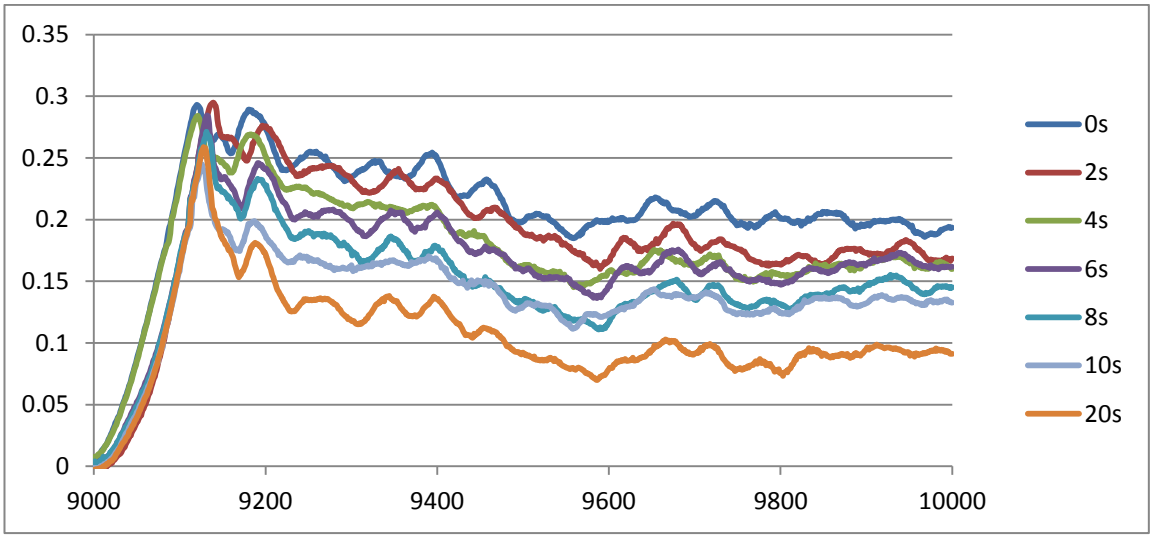

Figure 54 Friction levels with different on-time of lights. The effect on the kinetic friction is more significant than on the static friction.

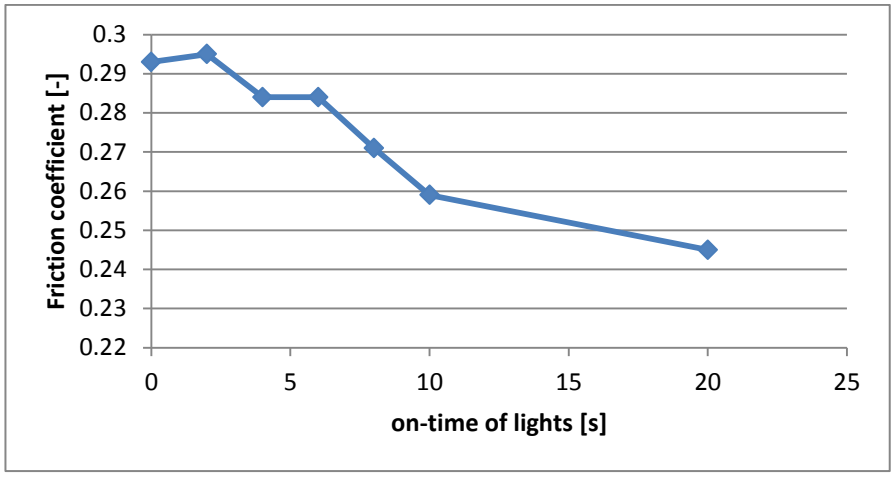

Figure 55 Static friction coefficient in function of on-time of lights

It can be noted that even few seconds on-time of the lights has a notable effect on kinetic friction levels. Four seconds of light on-time lowers the kinetic friction levels about 15% which indicates that the ice is warming up quite fast. However the static friction seems to hold its level better and changes are notable after 5 seconds on-time. This result suggests that for the kinetic friction tests lighting should be automatized to ensure as small and as even on-times as possible. On the other hand for the static friction tests the lighting on-time could be handled manually and the on-time should be under five seconds.

A repetition test was also performed to see how lighting effects on one individual lane that is lighted a run after another. For this test the MMR is set to perform 50 glides in a row and the track is lit for runs 1, 2, 5, 10, 20, 35 and 50. The lights were lit about 8 seconds before the target run and at that time the previous glide was initiating. After the lights were lit the MMR waited 2 minutes before the next glide. The results can be seen in Figure 56.

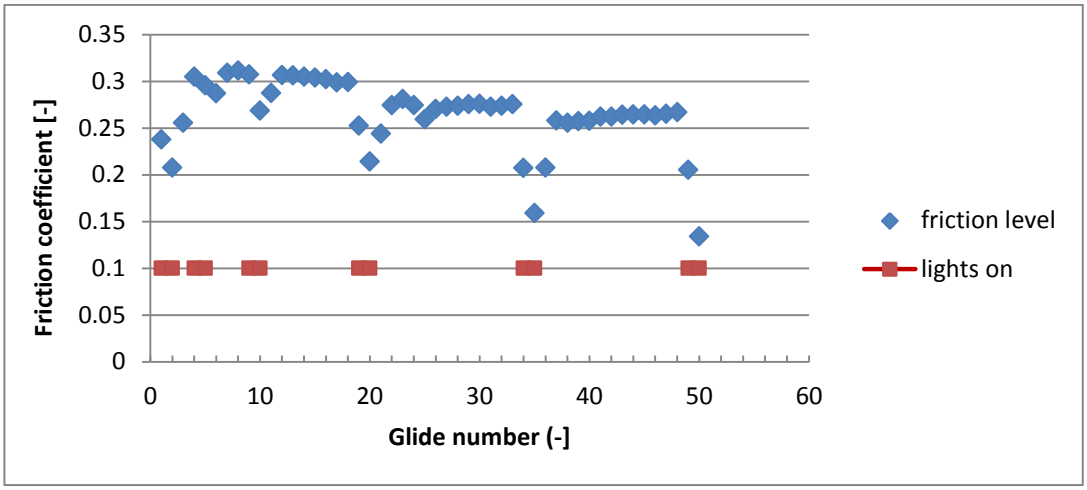

Figure 56 The friction level of repetitious tests on one line lighted occasionally. Red line shows when the lights were on.

It can be seen that the lights have a dramatic effect on the maximum friction level when repeatedly used on one measuring lane and this kind of measuring should be avoided.

6 Conclusions

The slip propagation of rubber ice contact was studied in this work. Phenomena at contact of a rubber sample and ice were observed using a high-speed camera, looking through the ice and the glass plate, onto which the ice was frozen. The phenomena that occurred in contact were then studied form captured sequence of images using digital image correlation or visually.

Sliding motion of a rubber sample does not initiate simultaneously in the whole contact area, but clear slip propagation occurs in contact. The detachment of the contact of a rubber sample initiates generally from the leading edge of the sample leading to a detachment front that swept through the contact area. With long dwell times (>10s) the detachment front can be detected from a sequence of images without digital image correlation, since the detached area changes its tone. This information could be used in preventing slip on some systems. The highest friction level is reached just after the detachment of the whole contact area, after which the friction drops to the kinetic friction level.

The results of this work shows that the precursors that occur during the friction build-up phase are related to events in contact area. However, clear precursors were noticed only with the hard rubber sample. The first precursor occurs when the first signs of detachment can be noticed. The second precursor can be found near the first signs of damage in the ice after long dwell times. This means that in some cases precursors at shear force data may be used as indicators of the initiation of the detachment.

It was noticed that the friction force depends logarithmically on the dwell, as has been suggested in earlier studies. Using long dwell times causes the friction coefficient to rise clearly above 1. Hard rubber and long (<30s) dwell time creates strong contact between rubber and ice, stronger than the shear strength of the ice. In these cases the sliding motion is initiated by breaking of the ice. Therefore the friction level cannot be raised infinitely, because the strength of the ice would be the weakest link. At short dwell times, even a small increase in dwell time increases friction notably, which could be taken into account when moving under slippery conditions on ice. Increasing the contact pressure decreased the friction coefficient also for longer dwell times.

The changes in temperature affected the static friction levels differently for different rubbers. The friction of the hard rubber increases when temperature was decreased as predicted.

However, the static friction of the soft rubber decreased when temperature decreased, which was not predicted.

The texturing of the rubber alters the propagation of the detachment front. Grooving of a sample stops or slows down the progress of the detachment, which moves the last contact point in the center of the sample. The measured static friction level was at least twice as high as the friction level of un-grooved sample.

Rubber texturing already exists in many rubber applications such as tires and shoes. However, the texturing is mostly done for resisting aquaplaning and gaining better grip on rough terrain. The consideration of preventing the slip propagation with texturing could lead to better grip, at least in ice contact, and should be studied further. The effect of texturing on slip propagation should also be tested on other surfaces such as tarmac and concrete, which are typical road pavements. Also more tests with texturing patterns used in this work should be done to make the results more statistically reliable.

Rubber texturing or its better invocation could increase friction of tire and shoe soles, which would lead to better performance and safety. This would save lives and mean savings in healthcare. The possibility of decreasing friction of rubber on ice with texturing could be beneficial for seals of machines that have to start in extremely cold conditions. Decreasing rubber friction on other surfaces with texturing would lead to increased efficiency of seals and windscreen wipers.

The results gave new insights into rubber ice contact and show that the Mini-Mu-Road combined with high-speed camera and digital image correlation is a powerful research tool for rubber research.

7 References

1 Brentin, Robert and Sarnacke, Phil. *rubber compounds - a market opprtunity study*. Omni Tech International, Midland, MI, 2011.

2 Strandroth, Johan, Rizzi, Matteo, Olai, Maria, Lie, Anders, and Tingvall, Claes. The effects of studded tires on fatal crashes with passenger cars and the benefits of electronic stability control (ESC) in Swedish winter driving. *Accident Analysis and Prevention*, 45 (2012), 50-60.

3 Crisman, Bruno and Roberti, Roberto. Tire wet-pavement traction management for safer roads. *Procedia - Social and Behavioral Sciences*, 53 (2012), 1055 – 1068.

4 Song, Xue-Guan, Wang, Lin, and Park, Young-Chul. Analysis and optimization of nitrile butadiene rubber. *Transactions of Nonferrous Metals Society of China*, 19 (2009), 220-224.

5 Koenen, A and Sanon, A. Tribological and vibroacoustic behavior of a contact between rubber and glass (application to wiper blade). *Tribology International*, 40 (2007), 1484-1491.

6 Yuchao, Ke, Xuefeng, Yao, Heng, Yang, and Xiaoyu, Liu. Kinetic friction characterizations of the tubular rubber seals. *TribologyInternational*, 72 (2014), 35-41.

7 Xu, Fangman, Yoshimura, Ken-ichi, and Mizuta, Hirotaka. Experimental study on friction properties of rubber material: Influence of surface roughness on sliding friction. (Kuala Lumpur 2013), Procedia Engineering.

8 Urbakh, Michael and Meyer, Ernst. Nanotribology: The renaissance of friction. *Nature Materials*, 9 (2010), 8-10.

9 Persson, B. Theory of rubber friction and contact mechanics. *Journal of chemical physics*, 115, 8 (August 2001).

10 Skouvaklis, Gerasimos, Blackford, Jane R, and Koutsos, Vasileios. Friction of rubber on ice: A new machine, influence of rubber properties and sliding parameters. *Tribology*

International, 49 (May 2012), 44-52.

11 Rantonen, Marko, Tuononen, Ari, and Sainio, Panu. Measuring stud and rubber friction on ice under laboratory conditions. *International Journal of Vehicle Systems Modelling and Testing*, 7 (2012), 194-207.

12 Fülöp, Tibor and Tuononen, Ari J. Evolution of ice surface under a sliding rubber block. *Wear 307* (2013), 52-59.

13 Bowden, F., Hughes, T. The mechanism of sliding on ice and snow. *Proceedings of the Royal Society of London. Series A: Mathematical and Physical Sciences 172 (949)* (1939), 280–298.

14 Tuononen, Ari. Digital Image Correlation to analyse stick–slip behaviour of tyre tread block. *Tribology International*, 69 (January 2014), 70-76.

15 Rubinstein, Shmuel M., Cohen, Gil, and Fineberg, Jay. Detachment fronts and the onset of dynamic friction. *Nature*, 430 (2004), 1005-1009.

16 Ben-David, Oded, Rubinstein, Shmuel M., and Fineberg, Jay. Slip-stick and the evolution of frictional strength. *Nature*, 463 (2010), 76-79.

17 Rubinstein, S, Cohen, G, and Fineberg, J. Dynamics of Precursors to Frictional Sliding. *Phys. Rev. Lett.*, 98 (June 2007), 226103-1-4.

18 Scholz, Christopher H. Earthquakes and friction laws. *Nature*, 391 (January 1998), 37-42.

19 Ben-Zion, Yehuda. Collective behaviour of earthquakes and faults: Continuum-discrete transitions, progressive evolutionary changes, and different dynamic regimes. *Reviews of Geophysics* (2008).

20 Asi, Ibrahim M. Evaluating skid resistance of different asphalt concrete mixes. *Building and Environment*, 42 (2007), 325-329.

21 Sukhorukov S., Løset S. Friction of sea ice on sea ice. *Cold Regions Science and Technology 94 1–12* (2013).

22 Kennedy, F.E., Schullson, E.M., Jones, D.E. The friction of ice on ice at low sliding velocities. *Philosophical Magazine A: Physics of Condensed Matter, Structure, Defects and Mechanical Properties 80 (5)* (2000), 1093–1110.

23 Kietzig, A.M., Hatzikiriakos, S.G., Englezos, P. Physics of ice friction. *Journal of Applied Physics 107 (8)* (2010).

24 Rosenberg, Robert. Why is ice slippery? *Physics today* (December 2005), 50-55.

25 Evans, D.C.B., Nye, J.F., Cheeseman, K.J. The kinetic friction of ice. *Proceedings of the Royal Society of London. Series A: Mathematical and Physical Sciences 347 (1651)* (1976), 493–512.

26 Oksanen, P., Keinonen, J. Mechanism of friction of ice. *Wear 78 (3)* (1982), 315–324.

27 Akkok, M., Ettles, C.M.M., Calabrese, S.J. Parameters affecting the kinetic friction of ice. *Journal of Tribology 109 (3)* (1987), 552–561.

28 H. Nyberg, S. Alfredson, S. Hogmark, and S. Jacobson. The asymmetrical friction mechanism that puts the curl in the curling stone. *Wear 301 (1-2)* (2013), 583-589.

29 Maeno, N., Arakawa, M.Adhesion shear theory of ice friction at low sliding velocities. Adhesion shear theory of ice friction at low sliding velocities, combined with ice sintering. *Journal of Applied Physics 95 (1)* (2004), 134–139.

30 Blackford, Jane R. Sintering and microstructure of ice: a review. *Journal of physics D: Applied physics*, 40 (2007), 355-385.

31 Makkonen, Lasse and Tikanmäki, Maria. Modeling the friction of ice. *Cold Regions Science and Technology*, 102 (2014), 84-93.

32 Hobbs, Peter V. *Ice Physics*. Oxford Classic Texts in the Physical Sciences, 1974.

33 Prinsenberg, S. and Peterson, I. K. Variations in Air-ice Drag Coefficient Due to Ice Surface Roughness. *International Journal of Offshore and Polar Engineering* (June 2002).

34 Treloar, L. R. G. *The physics of rubber elasticity*. Oxford Classic texts: in the physical science, New York, 1975.

35 Schweizer, B. and Wauer, J. Atomistic explanation of the Gough-Joule-effect. *The European physical journal B*, 23 (2001), 383-390.

36 Callister, William D. Jr. *Material science and engineering: An introduction*. John Wiley & sons, inc., USA, 1985.

37 greenwood. www.greenwood.wa.edu.au (Apr. 24, 2014).

38 Everaers, Ralf and Kremer, Kurt. Test of the Foundations of Classical Rubber Elasticity. *Micromolecules*, 28 (June 1995), 7291-7294.

39 Tuononen, Ari and Koisaari, Tapio. *Ajoneuvojen liikedynamiikka*. Autoalan koulutuskeskus, Helsinki, 2010.

40 Persson, B. N. J. Theory of rubber friction and contact mechanics. *Journal of chemical physics*, 115 (August 2001), 3840-3861.

41 Kärkimaa, Jukka. *Sliding friction of rubber on self-affine fractal surfaces*. Master's thesis, Helsinki, 2013.

42 http://insideracingtechnology.com/tirebkexerpt1.htm. Inside racing technilogy (Apr. 23, 2014).

43 Schulson, Erland M. and Fortt, Andrew L. Static strengthening of frictional surfaces of ice. *Acta Materialia*, 61 (January 2013), 1616-1623.

44 Fukahori, Y., Busfield, J. J. C., and Gabriel, P. How does rubber truly slide between Schallamach waves and stick–slip motion? *Wear*, 269 (August 2010), 854-866.

45 Rastogi, Pramod and Hack, Erwin. *Optical Methods for Solid Mechanics*. Wiley-VCH, Weinhein, Germany, 2012.

46 Sutton, Michael A., Orteu, Jean-José, and Schreier, Hubert W. *Image correlation for shape,*

Motionans Deformation Measurements. Springer, Columbia, USA, 2009.

47 Bossuyt, Sven. Aalto Research Day Proceedings. (Espoo 2013), Aalto University publication series.

48 Bossuyt, Sven. Optimized patterns for digital image correlation. (Taipei 2012).

49 Tuononen, Ari. Static friction coefficient of rubber on dry and wet glass: Influence of dwell time. In *Proceedings of the wear of materials conference* (Portland, USA 2013), Elsevier.

50 Ogden, R. W. and Roxburgh, D. G. A pseudo-elastic model for the Mullins effect in filled rubber. *Proceeding of the Royal society*, 455 (August 1999), 2861-2877.